Petroleum Research 11 (2026) 17–37

Contents lists available at ScienceDirect

Petroleum Research

journal homepage: http://www.keaipublishing.com/en/journals/petroleum-research/

Full Length Article

A quantification of the depositional–diagenetic heterogeneities in paleokarst hydrocarbon reservoirs: Sarvak Formation, Zagros Basin, Iran

Hamzeh Mehrabi *, Rakhshandeh Ataei, Vahid Tavakoli, Elham Talebi

School of Geology, College of Science, University of Tehran, Tehran, Iran

ARTICLE INFO

Article history:
Received 21 December 2024
Received in revised form
11 June 2025
Accepted 20 June 2025
Available online 26 June 2025

Keywords:
Reservoir heterogeneity
Coefficient of variation
Dykstra-Parsons
Sarvak Formation
Paleokarst
Abadan Plain

ABSTRACT

This study explores the depositional and diagenetic heterogeneities of the Sarvak Formation, a paleokarst carbonate reservoir in the Zagros Basin, Iran, using sedimentological, diagenetic, and statistical analyses. Petrographic studies and well log data, combined with methods like Winland rock type classification, hydraulic flow unit analysis, and Lorenz zonation, were used to assess reservoir properties at multiple scales. Two heterogeneity scales were identified: small-scale (millimeter to centimeter), driven by facies variations and diagenesis, and large-scale (meter), linked to facies transitions and sequence stratigraphy. Large-scale heterogeneities, particularly those tied to sequence stratigraphic boundaries, are traceable within third-order sequences and systems tracts. The highest-quality reservoir intervals, characterized by rudist-rich zones and dissolved shoal facies, are found beneath the Cenomanian–Turonian boundary, preserving youthful karst features. In contrast, non-reservoir intervals beneath the mid-Turonian disconformity exhibit collapsed features from prolonged subaerial exposure, forming an over-mature karst profile. Small-scale heterogeneities require further investigation within lower-order sequences for accurate prediction. This research integrates various analytical methods, providing a robust framework for understanding how depositional and diagenetic factors control reservoir quality, enhancing predictability in karstified carbonate systems for hydrocarbon exploration and development.

© 2025 Chinese Petroleum Society. Publishing services by Elsevier B.V. on behalf of KeAi Communications Co. Ltd. This is an open access article under the CC BY license (http://creativecommons.org/licenses/by/4.0/).

1. Introduction

Carbonate reservoirs are among the most significant oil and gas reservoirs globally, with over 80% of the reservoirs in the Middle East, including Iran, composed of carbonate formations (Alsharhan, 2014; Mehrabi, 2023). Reservoir quality and characteristics in carbonate reservoirs exhibit substantial variability due to their intricate sedimentary history and complex diagenetic processes (Mehrabi et al., 2023; Moore and Wade, 2013; Sadeghi et al., 2021). As a result, carbonate reservoirs display a higher degree of heterogeneity compared to clastic reservoirs (Ahr, 2008; Lucia, 2007).

Reservoir heterogeneity encompasses variations in petrophysical properties such as porosity, permeability, water saturation, and capillary pressure, which can arise from depositional processes, diagenetic alterations, and fractures (Ahr, 2008; Tiab and Donaldson, 2015). These heterogeneities occur at scales ranging from nanometers to kilometers and are crucial to understanding reservoir behavior (Mehrabi and Bagherpour, 2022; Tavakoli, 2020). Previous studies have shown that reservoir heterogeneities can be predicted within a sequence stratigraphic framework (Enayati-Bidgoli and Rahimpour–Bonab, 2016; Zahid et al., 2016; Foroshani et al., 2023; Fragoso et al., 2023; Jafarian et al., 2024). Quantifying these heterogeneities has been a key focus in carbonate reservoir studies (Fitch et al., 2015; Hosseinzadeh and Tavakoli, 2024; Song et al., 2020; Tavoosi Iraj et al., 2021; Xiao et al., 2022).

The Sarvak Formation is the second most important oil reservoir in Iran, after the Asmari Formation (Motiei, 1993). It is the most significant carbonate reservoir in the Abadan Plain, which has been the subject of numerous studies focusing on its sedimentological characteristics and reservoir properties. As such, it is crucial to study this formation from various perspectives,

* Corresponding author.
E-mail addresses: mehrabi.hamze@ut.ac.ir, hmehrabi.ut@gmail.com (H. Mehrabi).
Peer review under the responsibility of Editorial Office of Petroleum Research.

https://doi.org/10.1016/j.ptlrs.2025.06.003
2096-2495/© 2025 Chinese Petroleum Society. Publishing services by Elsevier B.V. on behalf of KeAi Communications Co. Ltd. This is an open access article under the CC BY license (http://creativecommons.org/licenses/by/4.0/).

including geological (Esrafili-Dizaji et al., 2015; Mehrabi et al., 2015; Mohseni and Zeybaram Javanmard, 2020; Rahimpour-Bonab et al., 2012a, 2013), petrophysical (Gholami Zadeh et al., 2019; Kiani et al., 2022; Mehrabi et al., 2020, 2023a), geochemical (Asadi Mehmandosti et al., 2013; Navidtalab et al., 2016; Abdolahi et al., 2024), and paleontological (Bagherpour et al., 2021) aspects. However, previous research has primarily relied on isolated approaches, such as facies analysis, diagenetic studies, or petrophysical evaluations, without integrating these methods to quantify reservoir heterogeneities comprehensively.

This study bridges this gap by combining descriptive sedimentological methods (e.g., facies analysis, diagenesis, and sequence stratigraphy) with reservoir rock classification techniques (e.g., Winland method, Hydraulic Flow Units, electrofacies, and Lorenz zonation) and statistical heterogeneity analysis (e.g., Coefficient of Variation and Dykstra–Parson's coefficient). By doing so, we provide a novel, multi-faceted understanding of the Sarvak Formation's reservoir heterogeneities, offering a more robust framework for characterizing and predicting reservoir performance. This integrated approach not only enhances our current knowledge of the Sarvak Formation but also sets a precedent for future studies aiming to quantify heterogeneity in complex carbonate reservoirs.

2. Geological setting

The study area for this research is the Abadan Plain, situated in the western part of the Zagros sedimentary basin (Fig. 1A). The focus of the study is the Sarvak Formation, which dates from the Late Albian to Early Turonian, with the upper part specifically corresponding to the Cenomanian–Turonian interval (Fig. 1B) (Omidvar et al., 2014; Mehrabi et al., 2022a, 2022b; Navidtalab et al., 2024). The Sarvak Formation is a significant hydrocarbon reservoir within the Bangestan Group (Rahimpour-Bonab et al., 2012a), characterized by a thick succession of platform carbonates that reflect a shallow marine depositional environment (Assadi et al., 2016). In the broader Middle East region, the Sarvak Formation correlates with the Mishrif Formation in Iraq, the Mauddud, Khatiyah (Ahmadi), and Mishrif formations in UAE and Qatar, and the Natih Formation in Oman (Alsharhan, 2014; Sadooni and Aqrawi, 2000). These equivalents share similar lithological and depositional characteristics, indicative of widespread carbonate platform development during the same geological period (Bromhead et al., 2022). In the Abadan Plain, the Sarvak Formation conformably overlies the Kazhdumi Formation, while its upper boundary with the Laffan/Ilam Formation is marked by an erosional discontinuity (Fig. 1B) (Mehrabi et al., 2023b).

During the Cenomanian–Turonian period, the study area (Zagros) was located on the northeastern margin of the Arabian Plate, near the equator at latitudes of approximately 4–5°, resulting in a hot and humid climate (Keller, 2008; Sharland et al., 2001). During this time, climatic conditions, sea-level fluctuations, the onset of the closure of the Neo-Tethys, basement fault activities, and the movement of Hormuz salt domes led to the formation of paleo-highs and regional unconformities within the Sarvak Formation and its stratigraphic equivalents across the Middle East (Alavi, 2004; Hollis, 2011; Madanipour et al., 2024; Mehrabi and Rahimpour-Bonab, 2014; Simmons et al., 2025; Razin et al., 2010; Sharp et al., 2010; van Buchem et al., 2011; Vergés et al., 2024).

The significant erosional discontinuity at the upper boundary of the Sarvak Formation, known as the middle Turonian discontinuity (mT-ES), along with other intraformational discontinuities, such as the Cenomanian-Turonian boundary discontinuity (CT-ES), has resulted in the erosion of this formation and altered its reservoir characteristics across much of the Zagros and Arabian Plate

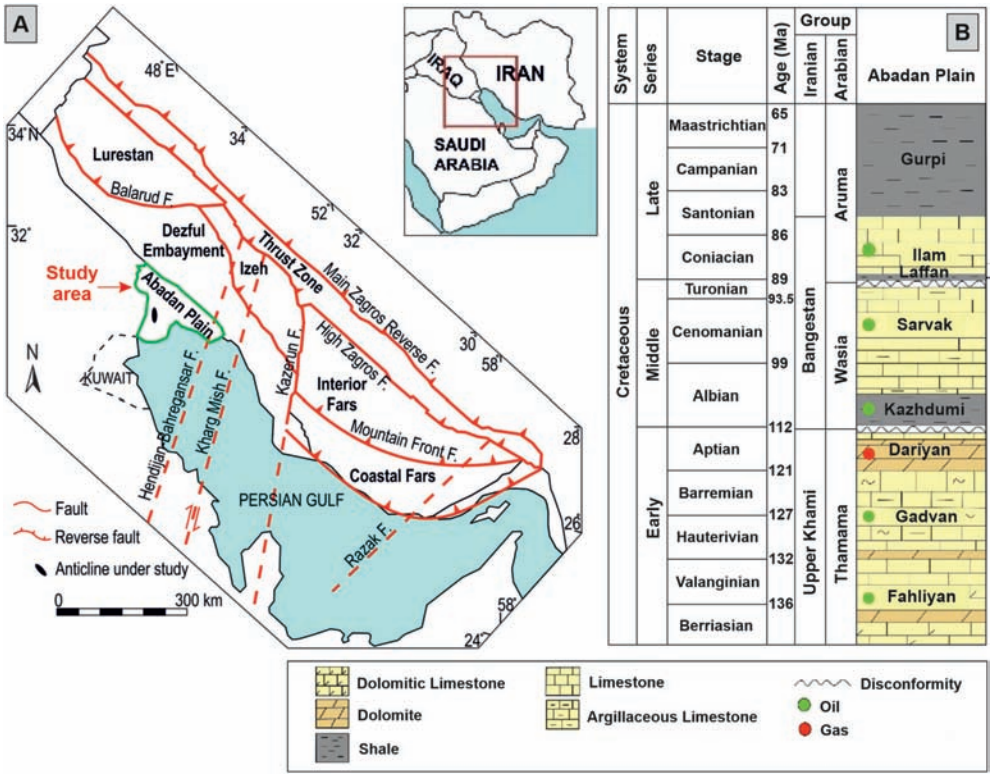


Fig. 1. A: Location map of the Abadan Plain in SW Iran reproduced after Sherkati and Letouzey (2004). B: Cretaceous stratigraphic chart of Abadan Plain. Stratigraphic position of the Sarvak Formation and its disconformities are shown (adopted with some modifications from (Mazdarani et al., 2023).

(Hajikazemi et al., 2010, 2012, 2017; Mehrabi et al., 2022a, 2022b; Abbasi et al., 2024). These discontinuities are associated with features such as karstification, brecciation, and the development of paleosol horizons (Hajikazemi et al., 2010; Malekzadeh et al., 2020; Mehdipour et al., 2023; Mehrabi et al., 2020).

3. Data and methods

The dataset for this study includes 258 m of core samples, 550 thin sections, porosity–permeability measurements (532 plug samples), and petrophysical logs (gamma-ray, resistivity, density, and neutron) from the Sarvak Formation in an oilfield in the Abadan Plain (Fig. 1A). To evaluate the composition and facies variability, comprehensive macroscopic and petrographic inspections were carried out on cores, slabs, plugs and thin-sections. Facies analysis was adopted using standard facies nomenclature schemes (i.e, Dunham, 1962; Embry and Klovan, 1971) and facies models (Flügel, 2013). The identification of depositional sequences was based on the transgressive–regressive (T–R) sequence stratigraphy method, as developed and described by Embry (2002) and Catuneanu et al. (2011).

The porosity-permeability dataset was initially screened to eliminate samples containing (micro)fractures. Specifically, samples with porosity values below 5% and permeability values exceeding 10 mD were excluded from the dataset prior to conducting the reservoir quality evaluation methods. Reservoir rock types, electrofacies and flow units were identified based on the following approaches:

i. The multi-resolution graph-based clustering (MRGC) method

The MRGC method in Geolog software, which combines hierarchical clustering with artificial intelligence, was applied in this study to analyze the electrofacies of the Sarvak Formation. This approach automatically determines the optimal number of clusters (Rabiller, 2005). The input logs, including gamma-ray (GR), sonic (DT), density (RHOB), and neutron (NPHI), are first preprocessed to ensure consistency and remove any outliers.

The MRGC method involves several mathematical concepts and formulae to determine electrofacies from well log data. While the exact implementation in Geolog Software may be proprietary, the general mathematical framework of MRGC can be described as follows (Equations (1)–(3)):

(1) Distance Metric Calculation

The similarity between data points (log measurements) is typically calculated using a distance metric, such as the Euclidean distance. For two data points x_i and x_j, the Euclidean distance d_{ij} is given by:

$$d_{ij} = \sqrt{\sum_{k=1}^{n} \left(x_{ik} - x_{jk}\right)^2} \quad (1)$$

where n is the number of input logs (e.g., GR, DT, RHOB, NPHI), and x_{ik} and x_{jk} are the values of the k-th log for points i and j, respectively.

(2) Graph Construction

A graph G=(V,E) is constructed, where V represents the nodes (data points) and E represents the edges weighted by the similarity (or distance) between nodes. The edge weight wij between nodes i and j can be defined using a kernel function, such as the Gaussian kernel:

$$w_{ij} = exp\left(-\frac{d_{ij}^2}{2\sigma^2}\right) \quad (2)$$

(3) Multi-Resolution Analysis

MRGC analyzes the graph at multiple resolutions by varying the scale parameter σ. This allows the algorithm to detect clusters at different levels of granularity, from fine (local) to coarse (global) structures.

(4) Cluster Identification

Clusters are identified by partitioning the graph based on connectivity and edge weights. This can involve spectral clustering techniques, where the graph Laplacian matrix L is computed:

$$L = D - W \quad (3)$$

where D is the degree matrix (a diagonal matrix with $D_{ii} = \sum_j w_{ij}$) and W is the adjacency matrix of edge weights. Eigenvalues and eigenvectors of L are then used to identify clusters.

(5) Electrofacies Assignment

Each cluster corresponds to an electrofacies, and the final assignment of data points to electrofacies is based on their membership in the identified clusters.

ii. Winland method

This method uses R35 values by using the following Equation (4) (Kolodzie, 1980):

$$\text{Log R35} = 0.732 + 0.588\ \text{Log (K)} - 0.864\ \text{Log (}\varphi\text{)} \quad (4)$$

In the formula, K represents permeability in millidarcies, while φ denotes porosity as a percentage.

iii. Hydraulic flow units (HFU) definition using the flow zone indicator (FZI)

This method was firstly presented by Amaefule et al. (1993) that uses porosity and permeability data to calculate the reservoir quality index (RQI), normalized porosity (PhiZ), and FZI (Equations (5)–(7)):

$$RQI = 0.0314\sqrt{(K/\varnothing e)} \quad (5)$$

$$\varnothing_z = \varnothing e/(1\text{-}\varnothing e) \quad (6)$$

$$FZI = RQI/\varnothing z \quad (7)$$

iv. Lorenz reservoir zonation

Gunter et al. (1997) proposed a method of reservoir zonation that incorporates porosity and permeability data to calculate the storage capacity (PhiH) and flow capacity (KH) (Equations (8) and

(9)):

$$KH_{cum} = K_1\,(h_1\text{-}h_0)/Kh_{total} + K_2\,(h_2\text{-}h_1)/Kh_{total} + \ldots. + Kn\,(h_n\text{-}h_{n\text{-}1})/Kh_{total} \quad (8)$$

$$PhiH_{cum} = \Phi_1\,(h_1\text{-}h_0)/\Phi h_{total} + \Phi_2\,(h_2\text{-}h_1)/\Phi h_{total} + \ldots. + \Phi n\,(h_n\text{-}h_{n\text{-}1})/\Phi h_{total} \quad (9)$$

In the above equations, (h) represents the depth difference (thickness) in meters, (K) denotes permeability in millidarcies, and (φ) represents porosity as a percentage. The results are then compared to determine the best method for final interpretation within the framework of sequence stratigraphy.

For the quantitative analysis of reservoir heterogeneities, two methods were used (Fitch et al., 2015):

(1) Coefficient of variation (CV)

The CV of porosity-permeability data in different units and sedimentary sequences of a formation serves as a measure of variability relative to the mean value, with various equations available for its calculation. According to this approach, a homogeneous area has a CV of zero, and this value increases with increasing heterogeneity (Elkateb et al., 2003).

The coefficient of variation, CV, is defined as (Equation (10)):

$$CV = \frac{\sqrt{Var}(K)}{E(K)} \quad (10)$$

where E(K) represents the expectation (mean) of the permeability random variable K, and Var(K) denotes its variance. The square root is assumed to be positive. In the case where permeability follows a log-normal distribution, $\ln(K) \sim N(\mu,\sigma^2)$, meaning the natural logarithm of K is normally distributed with mean μ and variance σ^2. Given that $E(K) = \exp(\mu+0.5\sigma^2)$ and $Var(K) = \exp(2\mu+\sigma^2)[\exp(\sigma 2)-1]$, the coefficient of variation simplifies to (Equation (11)):

$$CV = \sqrt{\exp\,(\sigma^{2)} - 1} \quad (11)$$

Thus, CV is independent of μ for log-normally distributed permeability (Lake and Jensen, 1991). CV quantifies the variability of permeability relative to its mean value. In a homogeneous medium, CV = 0. While CV is generally unbounded, for a dataset of n permeability measurements, the empirical coefficient of variation CV is constrained by $CV \leq \sqrt{n-1}$.

(2) Dykstra-Parsons (V_{DP})

The Dykstra-Parsons coefficient (V_{DP}) is a widely utilized metric for assessing reservoir heterogeneity, primarily focusing on permeability variations. In their foundational work, Dykstra and Parsons employed minipermeameter measurements to derive this coefficient. However, core plug permeability data are more commonly used, and in some cases, transient test data may also be applied (Johnson, 1956; Lake and Jensen, 1991). The procedure for estimating V_{DP}, as outlined by Dykstra and Parsons, involves organizing permeability data in descending order, assigning cumulative probabilities to each value, and plotting these on log-normal probability paper. A best-fit line is then drawn through the plotted points, with greater emphasis placed on the central data points if deviations from linearity are observed. This line represents an idealized reservoir model with a log-normal permeability distribution. From this line, the permeability values at the 84th percentile ($K_{0.84}$) and the median ($K_{0.50}$) are determined, which are subsequently used to calculate the coefficient (Equation (12)):

$$V_{DP} = \frac{K_{0.50} - K_{0.84}}{K_{0.50}} \quad (12)$$

Lower values of V_{DP} (ranging from 0 to 0.5) indicate minimal heterogeneity, whereas higher values (between 0.7 and 1.0) signify greater heterogeneity.

4. Results

4.1. Sedimentology

4.1.1. Facies analysis

The analysis of the skeletal and non-skeletal components, as well as the textures observed in thin sections of the Sarvak Formation, has led to the identification of eight sedimentary microfacies, each corresponding to different sub-environments. A summary of the facies characteristics of the Sarvak Formation is provided in Table 1, and microscopic images of the microfacies are shown in Fig. 2.

Table 1
Summarized facies characteristics of the Sarvak Formation in the studied field, Abadan Plain, Zagros, Iran.

Depositional setting	Standard microfacies (Flügel, 2010)	Energy level	Non-skeletal grains	Skeletal grains	Facies name	Facies code
Outer-ramp	RMF9	Low	Peloid	Planktic foraminifer, echinoderm, Oligostegina	Planktonic foraminifer microbioclast wackestone	**MF1**
Mid-ramp	RMF3	Variable	–	Planktic & benthic foraminifer. echinoderm, Bivalves	Foraminiferal (benthic and planktonic) bioclastic wackestone to packstone	**MF2**
Open marine lagoon	RMF17	Variable	Intraclast	Benthic foraminifer, echinoderms debris	Benthic foraminifer bioclast (echinoids) wackestone	**MF3**
Seaward-shoal	RMF26	High	Intraclast	Bivalves debris, rudist, coral, echinoderm	Bioclastic grainstone	**MF4**
Central-shoal	RMF27	High	–	Benthic foraminifer, bivalves debris, rudist, coral, green algae	Bioclast benthic foraminifera packstone to grainstone	**MF5**
Leeward-shoal	RMF13	Variable	Peloid	Benthic foraminifer	Benthic foraminifera peloidal wackestone to packstone	**MF6**
Reef-talus	RMF15	Variable	Intraclast	Bivalves, rudist. coral, green algae	Bioclast (rudist & coral) rudstone،floatstone	**MF7**
Lagoon	RMF16	Low	Peloid	Benthic foraminifer	Bioturbated benthic foraminifer peloidal mudstone to wackestone	**MF8**

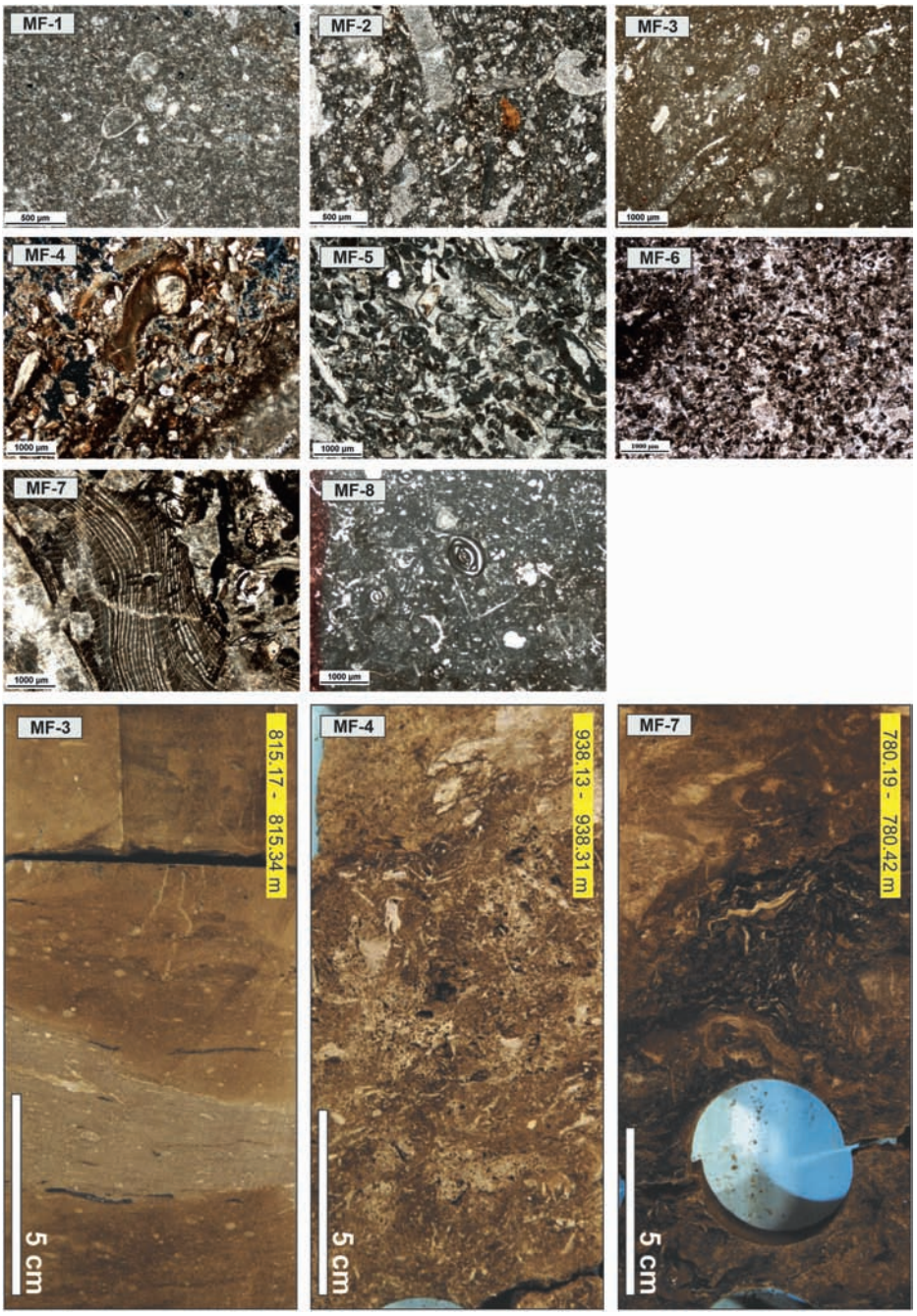


Fig. 2. Photomicrographs and core photos of depositional facies of the Sarvak Fm. in the Abadan Plain. MF-1: Planktonic foraminifera, microbioclast wackestone; MF-2: Foraminiferal (benthic and planktonic), bioclastic wackestone to packstone; MF-3: Benthic foraminifers, bioclast (echinoids) wackestone; MF-4: Bioclastic grainstone; MF-5: Bioclast, benthic foraminifera packstone to grainstone; MF-6: Benthic foraminifera, peloidal wackestone to packstone; MF-7: Bioclast (rudist–coral) rudstone‧floatstone; MF-8: Bioturbated benthic foraminifera, peloidal mudstone to wackestone.

4.1.1.1. MF1: planktonic foraminifer microbioclast wackestone. This facies exhibits a mud-dominated texture (wackestone) and is characterized by an abundance of planktonic foraminifera (e.g., *Globigerinoides*, *Hedbergella*, and *Rotalipora*), oligosteginids, and a diverse assemblage of bioclasts, including echinoderms, rudists, bivalves, sponge spicules, ostracods, and rare small benthic foraminifera (e.g., *Rotalia*). Peloids are also present as non-skeletal components (Fig. 2). The bioclasts are predominantly silt-sized, with echinoderm fragments being particularly abundant. This facies corresponds to RMF9 of Flügel (2013). The depositional environment is interpreted as a deep marine setting within a carbonate platform, based on the fine grain size (calcilutite to calcarenite), poor sorting, mud-supported fabric, and the presence of planktonic foraminifera. The dominance of planktonic biota, coupled with the scarcity of benthic foraminifera, suggests deposition in an outer ramp environment below the storm wave base (SWB) (Flügel, 2013).

4.1.1.2. MF2: foraminiferal (benthic and planktonic) bioclastic wackestone to packstone. This facies exhibits a spectrum of textures ranging from mud-dominated to grain-supported (wackestone to packstone) and contains a diverse assemblage of both

large and small benthic foraminifera (e.g., *Textularia* and *Rotalia*), planktonic foraminifera, rudists, bivalves, echinoderms, algae, and ostracods (Fig. 2). Additionally, peloids and rare intraclasts are present as non-skeletal components. The grain sizes vary widely, from silt to gravel, and the facies includes a mixture of benthic and planktonic fauna. Most bioclasts exhibit significant abrasion. This facies aligns with RMF3 of Flügel (2013). The coexistence of abraded bioclasts (indicative of high-energy conditions) within a mud-dominated texture (suggestive of low-energy conditions) is referred to as "textural inversion" in the literature (Flügel, 2013) and has been previously documented in the depositional facies of the Sarvak Formation in the Dezful Embayment (Mehrabi and Rahimpour-Bonab, 2014). Based on its stratigraphic position, association with open marine facies, and the described characteristics, the depositional environment of this facies is interpreted as a middle ramp setting (equivalent to a middle ramp in Flügel, 2013).

4.1.1.3. MF3: benthic foraminifer bioclast (echinoids) wackestone. This facies is characterized by a mud-dominated texture (wackestone) in which skeletal fragments and benthic foraminifera constitute the dominant allochems (Fig. 2). The benthic foraminifera include *Textularid* sp., *Dictyoconus pachymarginalis*, and *Orbitolina* sp., while skeletal debris comprises echinoderms, rudists, dasyclad algae, and bivalves. Non-skeletal components of this facies consist of intraclasts and peloids, with oligosteginids and sponge spicules occurring as subordinate grains (Fig. 2). The low abundance of planktonic foraminifera, coupled with the presence of benthic foraminifera and large fragments of rudists and echinoderms, suggests deposition in a shallower environment compared to the other two defined microfacies (i.e., MF-1 and MF-2). This facies can be correlated with RMF-7 (bioclastic wackestones and packstones with worn skeletal grains), which have been attributed to middle ramp environment (Flügel, 2013).

4.1.1.4. MF4: bioclastic grainstone. This grain-dominated facies is primarily composed of bioclasts, predominantly rudists, echinoderms, bivalves, and algal fragments. Additionally, small benthic foraminifera and peloids are present as subordinate components (Fig. 2). The allochems in this facies exhibit a calcarenite grain size with good sorting. A key characteristic of this facies is the abundance of highly abraded bioclasts and evidence of early (marine) cementation (Fig. 2). The grain-dominated texture indicates deposition under high-energy conditions. The predominance of bioclasts over benthic foraminifera and peloids, combined with the high degree of sorting and extensive isopachous cementation, suggests deposition in shoal complexes near the fair-weather wave base (FWWB). This facies can be correlated with RMF-26 (Bioclastic grainstone/packstone with diverse skeletal grains) in the ramp's standard microfacies and (Flügel, 2013). It is interpreted to have formed in the seaward portion of a shoal environment within the distal regions of the inner ramp (Bauer et al., 2002; Flügel, 2013).

4.1.1.5. MF5: bioclast benthic foraminifera packstone to grainstone. The primary distinctions of this facies from MF-4 (bioclastic grainstone) are the dominance of benthic foraminifera as the main allochems and the presence of lime mud as a matrix (ranging from <5% to 40% in frequency). The benthic foraminifera include *Nezzazata* sp., *Dicyclina schlumbergeri*, *Nezzazatinella picardi*, *Nummoloculina* sp., and *Textularids* sp., while skeletal fragments are predominantly composed of rudists, green algae, echinoderms, and other bivalves (Fig. 2). No significant sedimentary structures are observed in this facies. The grain-dominated textures suggest deposition under high-energy conditions. However, the majority of the allochems consist of shallow-marine (lagoonal) index fauna, such as hyaline benthic foraminifera, green algae, and rudists. The presence of variable amounts of lime mud as a matrix indicates a lower energy regime compared to MF-4. This facies corresponds to RMF27 of Flügel (2013), which is typical of high-energy, central-shoal environments. Similar facies are typically attributed to the central to leeward side of shoal complexes, where water energy levels and, consequently, marine cementation are reduced relative to the seaward shoal (Flügel, 2013).

4.1.1.6. MF6: benthic foraminifera peloidal wackestone to packstone. This facies is characterized by the dominance of peloids and small benthic foraminifera, including *Nezzazata* sp., *Dicyclina schlumbergeri*, *Nezzazatinella picardi*, *Nummoloculina* sp., and *Textularids* sp. Other components include rudists, bivalves, and green algae debris. Peloids are particularly abundant and constitute the primary allochems in most samples of this facies (Fig. 2). Evidence of bioturbation and micritization is also present. The facies exhibits a range of textures, from mud-to grain-dominated. Compared to MF-4 and MF-5, the mud-to grain-dominated textures of this facies suggest deposition under relatively lower energy conditions. The absence of fully preserved shells, along with the abundance of well-rounded, micritized bioclasts and intraclasts, indicates reworking (under high-energy conditions) and bioerosion in an environment likely situated around the fair-weather wave base (Korbar et al., 2001). It aligns with RMF13 of Flügel (2013), which is typical of leeward-shoal environments with variable energy. Consequently, the depositional setting of this facies is interpreted as the leeward parts of shoal complexes within the inner ramp. The predominance of peloids and benthic foraminifera over bioclasts, combined with low cementation rates and the presence of lime mud, further supports deposition in a leeward shoal setting (Flügel, 2013).

4.1.1.7. MF7: bioclast (rudist–coral) rudstone/floatstone. This facies is distinguished by the significant presence of rudists, corals, and green algae (Fig. 2). Lagoonal benthic foraminifera, such as *Nezzazata* sp. and miliolids, are also present, along with rare peloids and intraclasts as subordinate grains. Large (>2 mm in diameter) fragments of reef-building organisms, including rudists, corals, and algae, contribute to the mud-to grain-dominated textures, classified as floatstone and rudstone according to the textural classification scheme of Embry and Klovan (1971). This facies corresponds to RMF15 of Flügel (2013). In some instances, the occurrence of rudist rudstones and floatstones (on a macroscopic scale) is interpreted as rudist patch reefs (Di Stefano and Ruberti, 2000). The presence of a diverse and abundant stenohaline fauna, such as rudists and benthic foraminifera, suggests development in moderate-energy environments (Spalluto, 2012). Rudist colonies typically thrived in the shallower parts of the ramp (i.e., inner ramp) above the fair-weather wave base (FWWB) (Cestari and Sartorio, 1995). These facies are interpreted as talus deposits that formed around rudist-algal patch reefs. Similar facies have been documented in Upper Cretaceous sedimentary sequences across the Middle East and globally (e.g., Aqrawi et al., 2010; Esrafili-Dizaji et al., 2015; Rahimpour-Bonab et al., 2012a; Sadooni, 2005).

4.1.1.8. MF8: Bioturbated benthic foraminifer peloidal mudstone to wackestone. This mud-dominated microfacies is primarily characterized by large benthic foraminifera, including *Nezzazata* sp., alveolinids, *Dicyclina* sp., and miliolids, along with subordinate green algae, rudists, and gastropod fragments (Fig. 2). Peloids are the sole non-skeletal component present. Bioturbation is a significant sedimentary feature observed in this facies (Fig. 2). The high proportion of micrite, reflected in wackestone and mudstone

textures, indicates deposition in a low-energy environment. Based on the fossil content and sedimentary textures, a low-energy, shallow marine setting is inferred. The limited faunal diversity further supports restricted water circulation, consistent with a lagoonal environment (Bauer et al., 2002; Flügel, 2013). This facies aligns with RMF16 of Flügel (2013), which is typical of low-energy lagoon environments. These environments are typically defined by specific parameters, such as mud-dominated fabrics, abundant benthic foraminifera, green algae, gastropods, and bivalves (Flügel, 2013; Tucker and Wright, 1990).

In summary, the depositional facies of the Sarvak Formation were deposited across a range of subenvironments, including the inner ramp, middle to outer ramp settings. Within the inner ramp, facies include restricted lagoonal deposits (MF8), rudist reefs and their associated talus facies (MF7), and shoal deposits (MF4, MF5, MF6). Open marine lagoon facies are represented by wackestones containing benthic foraminifera and skeletal fragments, particularly echinoderm remains (MF3). In the middle and outer ramp settings, facies consist of wackestones and packstones with planktonic foraminifera and small skeletal fragments (MF1, MF2).

4.1.2. Diagenesis

Petrographic analysis of drilling cores and microscopic thin sections indicates that the Sarvak Formation has experienced a variety of diagenetic processes. These processes encompass dolomitization, mechanical and chemical compaction, micritization, silicification, dissolution, cementation (including equant, blocky, dolomitic, isopachous, and syntaxial cements), as well as brecciation and fracturing. Fig. 3 highlights the most prominent diagenetic processes identified in the Sarvak Formation. Below, summarized descriptions of the major diagenetic processes that significantly influence reservoir heterogeneity in the Sarvak Formation are provided.

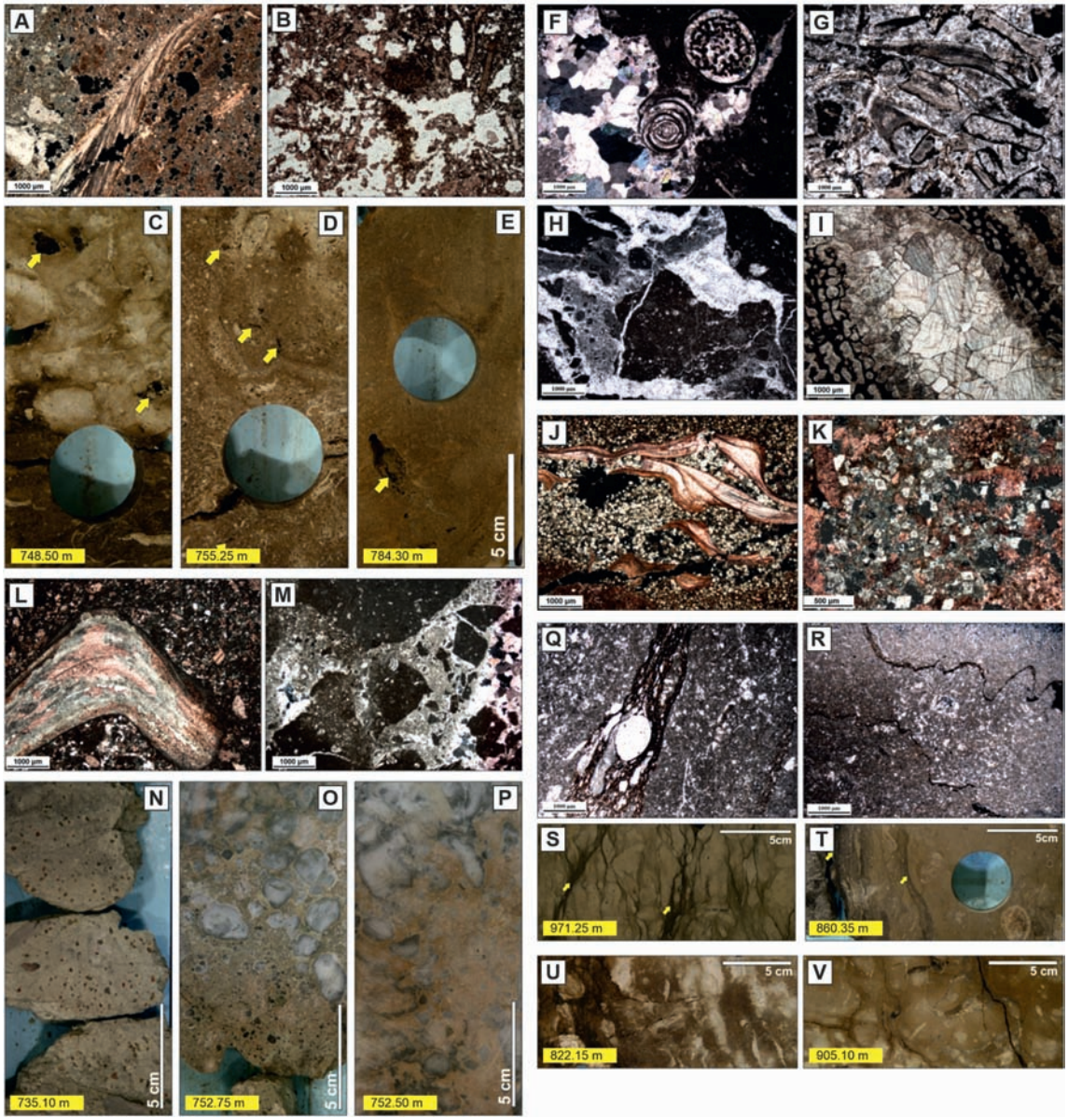


Fig. 3. Thin-section images and core photos of important diagenetic features of the Sarvak Formation in the studied fields in the Abadan Plain. A–E: dissolution; F–I: calcite cementation; J–K: dolomitization; L: silicification; M: brecciation; N–P: brecciation and paleosol; Q–T: chemical compaction; U–V: fracturing. A, F, J, K and M in XPL.

4.1.2.1. Cementation. This process represents one of the most significant diagenetic alterations in the studied formation, leading to the occlusion of both primary and secondary pore spaces. Interparticle, intraskeletal, moldic, and fracture pores are often partially or completely filled by cements. Calcite is the predominant cement phase, although dolomite is also present. The main types of cements identified include:

Isopachous cements are primarily observed in high-energy facies (packstones and grainstones) of shoal settings, where higher water circulation (and energy levels) in grain-supported facies results in more extensive isopachous cementation (e.g., MF-4; Fig. 3). In the studied interval, the frequency of isopachous cements is visually estimated to range from <5% to 20% in shoal facies.

Equant sparry cements are predominantly observed in rudist-dominated facies (floatstones to packstones) of reef-talus settings (e.g., MF-7). In these facies, equant cements commonly fill intergranular pore spaces and, in some cases, skeletal molds and large fractures (Fig. 3). The frequency of equant sparry cements is visually estimated to range from <5% to >40% in dissolved and cemented facies.

Coarse sparry (blocky) cements are commonly observed in reef-talus facies (MF-7). These cements often fill large vugs and rudist molds, particularly within meteorically dissolved intervals located beneath paleo-exposure surfaces (Fig. 3). The frequency of blocky cements is visually estimated to range from <5% to 35%. They also serve as the primary fracture-filling cement.

Syntaxial cements are primarily observed in MFs 2 and 3 and, to a lesser extent, in MF-4. They are mainly recorded as overgrowths around echinoderm debris in open marine and high-energy shoal facies (Fig. 3). The frequency of syntaxial cements is visually estimated to be <5% in these facies.

4.1.2.2. Dissolution. Meteoric dissolution is a widespread phenomenon in the upper part of the Sarvak Formation, manifesting as dissolution vugs and molds on both microscopic and macroscopic scales. Micro-karstic networks consist of isolated, fabric-selective vugs and interconnected, non-fabric selective vugs, which may be empty or partially to completely filled by various types of meteoric or burial cements (Fig. 3). This dissolution process predominantly affects high-energy shoal facies and reef-talus facies of the Sarvak Formation, occurring below paleoexposure surfaces.

4.1.2.3. Dissolution-collapsed brecciation. In the studied wells, brecciation is prominently observed beneath the Cenomanian–Turonian (C–T) boundary unconformity, evident on both macroscopic and microscopic scales (Fig. 3). The breccias are characterized by a clay-rich, reduced matrix, and in some samples, Fe-oxide staining imparts a pink coloration (Fig. 3). Silicification is also documented within the meteorically altered intervals, typically replacing bioclasts (e.g., rudists) and filling borings or intraskeletal pores as cement.

4.1.2.4. Dolomitization. In the Sarvak Formation, the dolomites are predominantly stylolite-related. The prevalence of mud-dominated facies and the greater burial depths of these intervals have facilitated intensive stylolitization and subsequent stylolite-related dolomitization (Fig. 3). This diagenetic process, particularly in mud-dominated facies (MFs 1, 2, 3, and MF-8; Table 1), has resulted in the development of high-quality reservoir intervals (see Rahimpour-Bonab et al., 2012b).

4.1.2.5. Compaction. This study demonstrates that the studied interval of the Sarvak Formation has been significantly influenced by compaction during and after burial, with the current burial depth reaching approximately 3 km in the studied wells. Compaction features in this formation can be categorized into two main types (Fig. 3): Mechanical compaction is primarily observed in grain-dominated facies of reef-talus and shoal complexes, manifesting as grain deformation and breakage (Fig. 3). Chemical compaction, also known as pressure dissolution, are recorded in the Sarvak Formation carbonates in the forms of both stylolites and solution seams (Fig. 3). Solution seams are more prevalent and are primarily found in mud-dominated facies (mudstones and wackestones), while stylolites are mainly observed in grain-supported facies of MFs 1, 2, 3, and 8 (Table 1).

4.1.2.6. Fracturing. Fractures are identified as significant post-depositional (diagenetic) features in the Sarvak Formation. In many instances, fractures are either completely or partially filled by calcite cements, although open fractures are also present. Micro-fractures have been documented during thin section studies (Fig. 3). In numerous cases, fracturing postdates the aforementioned diagenetic processes. Fracturing appears to play a major role in hydrocarbon production from the Sarvak Formation in the studied wells. The highest frequency of fractures is observed in the lower parts of the formation. A significant proportion of the fractures are likely natural, as evidenced by their varying degrees of cementation.

The examination of textural relationships and their interpretation indicates that the Sarvak Formation has been influenced by a range of diagenetic processes across various environments. These include marine processes such as isopachous cementation, bioturbation, and micritization; meteoric processes such as intense dissolution, dissolution-collapsed brecciation, paleosol formation, silicification, drusy calcite cementation, and recrystallization; shallow burial processes such as equant and syntaxial calcite cementation, mechanical compaction, and recrystallization; and deep burial processes such as blocky calcite cementation, stylolitization and stylolite-related dolomitization, fracturing, pyritization, and recrystallization.

4.1.3. Sequence stratigraphy

The integration of findings from sedimentary facies analysis, diagenetic processes associated with sequence boundaries (including diagenetic features linked to unconformities, such as dissolution and meteoric cementation), and well-log data has led to the identification of two third-order sedimentary sequences within the Sarvak Formation. Each sequence is composed of two systems tracts: a regressive systems tract (RST) and a transgressive systems tract (TST). Biostratigraphic studies have determined that the first sequence, labeled as Sv_Cen in Fig. 4, corresponds to the Cenomanian, while the second sequence, labeled as Sv_Tur, corresponds to the Turonian (see Bagherpour et al., 2021; Mehrabi et al., 2020; Omidvar et al., 2014). The distinct sequences within the Sarvak Formation, along with their associated facies and diagenetic characteristics, are depicted in Fig. 4.

4.1.3.1. Cenomanian sequence (Sv_Cen). This sequence has a total thickness of 245 m in the studied field. Within the transgressive systems tract (TST) of this sequence, the predominant facies include outer ramp (MF1) and open marine lagoon (MF3). The key diagenetic processes observed in this systems tract are dolomitization associated with stylolites, mechanical and chemical compaction, and, to a lesser extent, burial cements. The maximum flooding surface (MFS) is characterized by the deepest facies of the middle to outer ramp. The MFS of this sequence corresponds to the MFS K130 of Sharland et al. (2001). In the regressive systems tract (RST), the sequence is dominated by facies associated with reef

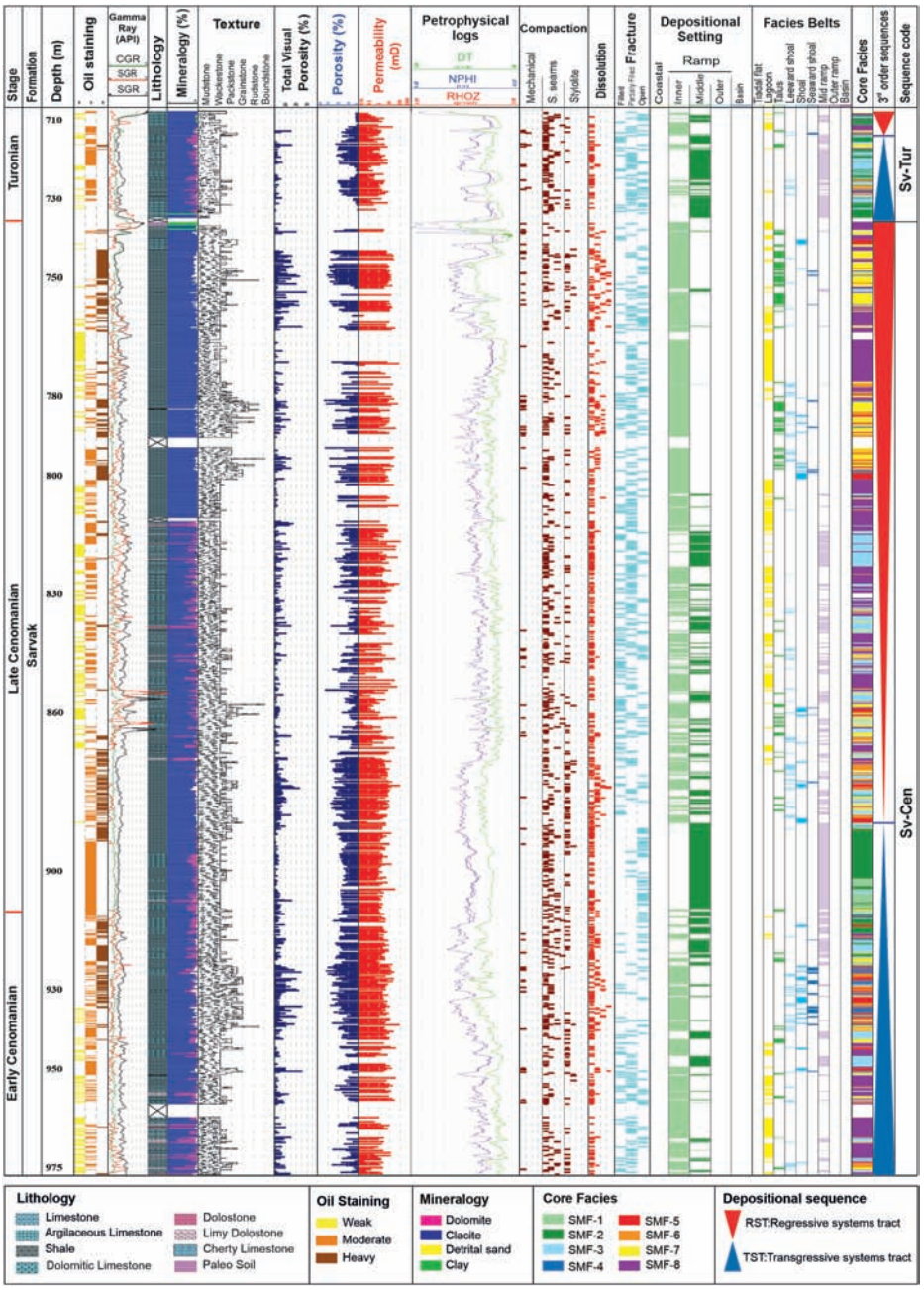


Fig. 4. Sedimentological log of the Sarvak Formation in the studied well, Abadan Plain.

talus (MF7) and restricted lagoons (MF8). The primary diagenetic processes in this tract include meteoric diagenesis, marked by extensive dissolution, meteoric cementation, silicification, and some degree of compaction. The sequence is capped by a paleo-exposure surface. Diagenetic features below this surface, such as extensive meteoric dissolution, meteoric cements, iron oxide staining, and silicification, indicate that this is the maximum regressive surface (MRS).

4.1.3.2. Turonian sequence (Sv_Tur). This sequence has a total thickness of 30 m in the studied field. Within the transgressive systems tract (TST) of this sequence, the dominant facies are middle ramp (MF2) and open marine lagoon (MF3). The primary diagenetic processes in this systems tract include dolomitization associated with stylolites, mechanical and chemical compaction, and, to a lesser extent, burial cements. The MFS is characterized by the expansion of seaward shoal facies (MF4). The MFS of this sequence corresponds to the MFS K140 of Sharland et al. (2001). In the RST, the sequence primarily consists of facies related to shallow marine environments and restricted lagoons (MF8). The main diagenetic processes observed in this tract are meteoric diagenetic features, including extensive dissolution, meteoric cementation, silicification, and some compaction. The upper boundary of this sequence is marked by a disconformable surface. Diagenetic features below this disconformity, such as extensive meteoric dissolution, meteoric cements, thin soil horizons, iron oxide staining, and silicification, indicate that it is the maximum regressive surface (MRS).

Sequence stratigraphic analysis of the Sarvak Formation has been extensively investigated in various regions of the Zagros area, including the Dezful Embayment (Mehrabi et al., 2022a, 2022b), Lurestan (Mohseni and Zeybaram Javanmard, 2020), the Fars Zone (Gholami Zadeh et al., 2019), the Izeh Zone (Kalanat et al., 2021), the

Persian Gulf (Mehrabi, 2023), and the Abadan Plain (Assadi et al., 2016). These studies consistently identified two third-order depositional sequences within the upper Sarvak Formation. Age determination based on biostratigraphic and strontium isotope stratigraphic analyses reveals that these sequences correspond to the Cenomanian and Turonian stages, marked by two regional paleoexposure surfaces at the top of each sequence: (i) the mid-Turonian unconformity (mT-ES), which is widely traceable across the Middle East and the Tethyan realm, and (ii) the Cenomanian–Turonian boundary (CT-ES) disconformity, which is regionally extensive throughout the Middle East (see Mehrabi et al., 2022a, b; Navidtalab et al., 2024; Simmons et al., 2025). These sequences exhibit strong correlation with the reference sequence stratigraphic frameworks established for the Arabian Plate (e.g., Razin et al., 2010; Sharland et al., 2001).

4.2. Reservoir properties

4.2.1. Pore types

In this study, the reservoir rock pore system was initially characterized by distinguishing pore types through petrographic analysis, which included the examination of drill cores and thin sections. Following this, the Winland calculation method was applied. Using this method, R35 values—representing the pore throat radius at 35% mercury saturation—were calculated based on porosity and permeability data (Fig. 5A and B). These values were subsequently plotted on the standard Winland chart, allowing for the identification of seven distinct rock types based on iso-pore-throat lines (Fig. 5A and B). The average, minimum, and maximum porosity and permeability values for each Winland rock type (WRT) are summarized in Table 2. The results reveal that WRT-1 has the poorest reservoir quality, with an average porosity of 6.42% and an average permeability of 0.04%, while WRT-7 demonstrates the best reservoir quality, with an average porosity of 10.40% and an average permeability of 253.9%.

4.2.2. Hydraulic flow units

Using the relationships outlined in the data and methods section and employing a normal probability (cumulative) plot of FZI values, eleven hydraulic flow units (HFUs) were identified within the Sarvak Formation (Fig. 5A). The cumulative probability plot, along with cross-plots of porosity versus permeability and RQI versus PhiZ (normalized porosity), was utilized to differentiate the identified hydraulic flow units, as illustrated in Fig. 5A–C. The statistical ranges, including minimum, maximum, and average porosity and permeability values for each hydraulic flow unit, are presented in Table 3. The data indicate that reservoir quality

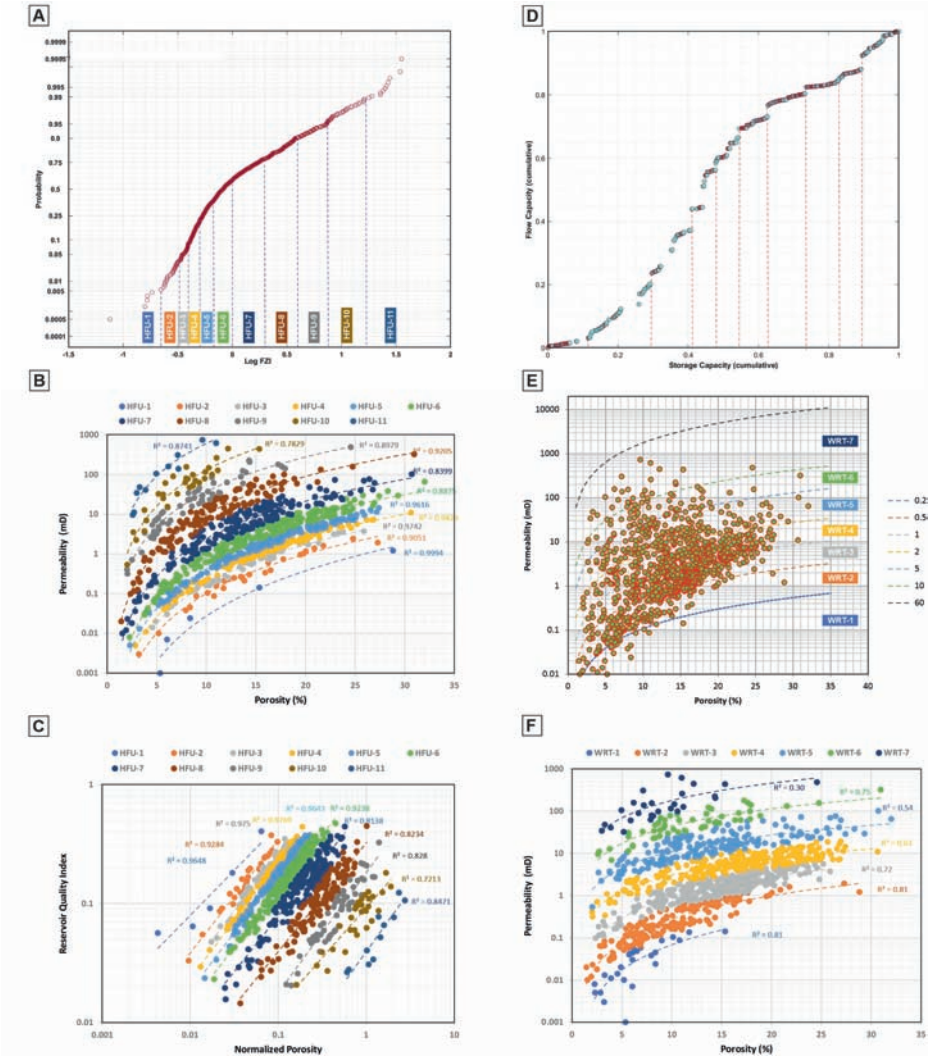


Fig. 5. Probability plot of Log FZI values (A), porosity–permeability plot (B) and normalized porosity vs. RQI for defined HFUs (C) of the Sarvak reservoir in the studied field. Cumulative chart of KH vs. PHIH values for defining the reservoir zones in the Lorenz method (D). Winland standard diagram for defining the WRTs (E) and porosity–permeability cros plot of defined Winland rock types (F) are also shown.

Table 2
Statistical parameters of minimum, maximum, and average of porosity–permeability data in the hydraulic flow units (HFUs) defined in the Sarvak Formation, Abadan Plain, Zagros, Iran.

WRT No.	Mean Porosity (%)	Mean Permeability (mD)	Mean RQI	Mean FZI	Mean R35	Reservoir Quality
1	6.49	0.04	0.02	0.35	0.14	Poor
2	10.43	0.38	0.05	0.54	0.35	Poor
3	14.48	1.88	0.11	0.72	0.73	Fair
4	16.12	6.11	0.19	1.24	1.39	Fair
5	14.03	19.61	0.35	2.77	3.07	Good
6	11.81	63.20	0.68	6.43	6.98	Good
7	9.19	199.16	1.34	16.06	16.73	Good

Table 3
Statistical parameters of minimum, maximum, and average of porosity–permeability data in the Winland rock types (WRTs) identified in the Sarvak Formation, Abadan Plain, Zagros, Iran.

HFU No.	Mean Porosity (%)	Mean Permeability (mD)	Mean RQI	Mean PhiZ	Mean FZI	Reservoir Quality
1	12.79	0.28	0.03	0.16	0.15	Poor
2	14.25	0.53	0.05	0.17	0.28	Poor
3	14.18	0.83	0.06	0.17	0.37	Poor
4	15.04	1.57	0.08	0.18	0.45	Good
5	16.24	3.13	0.11	0.20	0.57	Good
6	15.00	5.38	0.15	0.18	0.80	Excellent
7	13.42	10.57	0.22	0.16	1.37	Excellent
8	10.47	22.13	0.34	0.12	2.83	Excellent
9	8.76	48.35	0.54	0.10	5.65	Fair
10	7.61	89.62	0.88	0.08	10.67	Fair
11	5.59	200.14	1.46	0.06	25.64	Fair

improves progressively from HFU1 to HFU11, with HFUs 1 to 3 having the lowest average porosity (HFU1: 12.79%, HFU2: 14.25%, HFU3: 14.18%) and permeability (HFU1: 0.28mD, HFU2: 0.53mD, HFU3: 0.83mD), HFUs 4 and 5 showing good reservoir quality representing by moderate values of average porosity (HFU4: 15.04%, HFU5: 16.24%) and average permeability (HFU4: 1.57mD, HFU5: 3.13mD), HFUs 6 to 8 having excellent reservoir properties marked by highest values of average porosity (HFU6: 15%, HFU7: 13.42%, HFU8: 10.47%) and average permeability (HFU6: 5.38mD, HFU7: 10.57mD, HFU8: 22.13mD), and HFUs 9 to 11 exhibiting the low average porosity (HFU9: 8.76%, HFU10: 7.61%, HFU11: 5.59%) but highest average permeability (HFU9: 48.35mD, HFU10: 89.62mD, HFU11: 200.14mD).

4.2.3. Lorenz zonation

In this study, the storage capacity (PhiH) and flow capacity (KH) values were calculated using established mathematical relationships. A normal probability plot of these values was then generated, and based on the identified breakpoints in the plot, distinct Lorenz zones were delineated in the Sarvak Formation (Fig. 5C). The sedimentological characteristics and reservoir quality of each identified zone are summarized in Table 4. According to the Lorenz method, a formation can be classified into four categories of zones:

(1) Reservoir zones: High KH and high PhiH, such as zones 2, 3, 7, 8, and 10.
(2) Baffle zones: Low KH and high PhiH, such as zones 1 and 6.

Table 4
Statistical parameters calculated for Lorenz zones differentiated in the Sarvak Formation, Abadan Plain, Zagros, Iran.

Lorenz zones	Thickness (m)	Dominant facies	Dominant diagenesis	KH (cum%)	PhiH (cum%)	Dominant WRT	Dominant HFU	RPS (average)	R35	Zone type
Z1	38.1	MF2, MF3	Solution seam, Stylolite-related dolomitization, Micritization, Dissolution	5.44	13.43	2, 3	3 to 6	45.89	1.32	Baffle Unit
Z2	34.87	MF7, 8	Dissolution, Fracturing	14.76	15.85	4, 5	6 to 11	20.15	3.16	Reservoir Unit
Z3	34.82	MF7, 8	Dissolution	24.28	14.80	5 to 7	4 to 9	17.25	2.66	Reservoir Unit
Z4	10.78	MF3, 8	Dissolution. Stylolite-related dolomitization	11.77	3.67	1 to 4	1 to 3	51.43	4.34	Barrier Unit
Z5	27.17	MF3, 8	Stylolite-related dolomitization	13.18	7.44	6, 7	9 to 11	22.82	2.90	Speed Zone
Z6	23.84	MF3	Dissolution. Stylolite-related dolomitization	3.63	7.36	3, 4	3 to 5	78.62	1.47	Baffle Unit
Z7	25.18	MF2	Dissolution	7.29	10.54	4 to 7	5 to 9	90.87	1.53	Reservoir Unit
Z8	25.41	MF1, 2, 3	Dissolution, Stylolite-related dolomitization, Solution seam	6.24	11.51	5 to 7	4 to 8	55.21	1.29	Reservoir Unit
Z9	9.91	MF6	Dissolution. Micritization	1.44	4.64	1 to 3	1 to 4	34.20	1.21	Barrier Unit
Z10	38.02	MF8	Dissolution, Stylolite-related dolomitization	11.93	10.75	4 to 6	6 to 9	14.82	2.55	Reservoir Unit

Table 5
Summarized characteristics of electrofacies (EFs) defined in the Sarvak Formation, Abadan Plain, Zagros, Iran.

Electrical Facies	Dominant/Main Facies	Key Diagenetic Processes	Average Porosity (%)
1	SMF8	Solution seams, bioturbation	–
2	SMF3, SMF7, SMF2	Stylolite-related dolomites, stylolitization, dissolution, neomorphism, micritization, brecciation, mechanical compression, drilling effects	17.08
3	SMF3	Stylolite-related dolomites, dissolution, solution seams, mechanical compression, micritization, silicification, bioturbation	15.48
4	SMF3, SMF2, SMF1, SMF8	Stylolite-related dolomites, dissolution, fractures, brecciation, neomorphism, micritization, silicification, bioturbation	11.78
5	SMF7, SMF6, SMF3, SMF8	Stylolite-related dolomites, dissolution, neomorphism, micritization, fractures, silicification, bioturbation	7.1
6	SMF7, SMF8	Stylolite-related dolomites, dissolution, solution seams, mechanical compression, fractures, neomorphism, bioturbation	2.23
7	SMF3, SMF8	Stylolite-related dolomites, dissolution, brecciation, fractures, mechanical compression, micritization, drilling effects	7.35

(3) Barrier zones: Low KH and low PhiH, such as zones 4 and 9.
(4) Speed zones: High KH and low PhiH, such as zone 5 (further details in Table 4).

4.2.4. Electrofacies

Using the MRGC method and gamma-ray, neutron, density and sonic logs as inputs, seven electrofacies were identified in the Sarvak Formation. The sedimentologic characteristics, including dominant facies, diagenetic features, and reservoir quality of these electrofacies, are summarized in Table 5. Detailed statistical information for these electrofacies is provided in Table 6. Crossplots of petrophysical logs classified according to the electrofacies are shown in Fig. 6. Some overlaps are observed in the electrofacies data, as illustrated in Fig. 6, indicating methodological limitations in the classification approach.

4.3. Statistical analysis of reservoir heterogeneities

To quantitatively assess heterogeneities, two statistical methods were utilized: the Coefficient of Variation (CV) and the Dykstra-Parsons coefficient (VDP). Table 7 presents an example of the statistical calculations for these coefficients, specifically for one of the hydraulic flow units (HFU9) and the porosity parameter.

Table 6
Statistical parameters (min, max, average) of petrophysical logs calculated for the electrofacies identified in the Sarvak Formation.

E7	E6	E5	E4	E3	E2	E1	Electrofacies
0.008	−0.001	0.003	0.06	0.04	0.11	0.13	**NPHI (MIN)**
0.16	0.07	0.20	0.27	0.37	0.29	0.43	**NPHI (MAX)**
0.06	0.01	0.07	0.13	0.14	0.18	0.26	**NPHI (AVR)**
7.20	8.11	5.58	7.53	12.78	9.24	28.59	**CGR (MIN)**
34.93	33.30	29.80	21.68	51.66	33.18	55.81	**CGR (MAX)**
16.49	17.40	14.06	15.01	33.41	16.14	44.17	**CGR (AVR)**
52.89	48.76	52.74	53.91	54.25	61.13	65.06	**DT (MIN)**
71.35	60.58	71.82	74.14	85.09	85.08	95.57	**DT (MAX)**
60.33	54.51	60.25	65.55	68.30	71.47	78.20	**DT (AVR)**
3.80	4.68	3.80	3.67	2.98	3.80	2.67	**PEF (MIN)**
5.26	5.81	5.28	5.39	5.05	5.23	4.79	**PEF (MAX)**
4.80	5.07	4.85	4.78	4.49	4.63	3.72	**PEF (AVR)**
2.24	2.59	2.39	2.38	2.17	2.29	2.15	**RHOB (MIN)**
2.74	2.79	2.75	2.65	2.73	2.54	2.80	**RHOB (MAX)**
2.59	2.69	2.58	2.50	2.60	2.43	2.57	**RHOB (AVR)**
28.95	15.71	14.65	14.38	31.99	14.75	55.49	**SGR (MIN)**
106.88	53.03	49.68	49.31	74.25	43.56	79.77	**SGR (MAX)**
48.32	32.11	32.66	30.02	51.82	25.78	69.33	**SGR (AVR)**

4.3.1. Coefficient of variations (CV)

Based on the statistical and mathematical relationships outlined in the methods section, the CV values for porosity and permeability across all data were calculated, with the results summarized in Table 8 and depicted in Fig. 7. In this analysis, lower CV values indicate greater homogeneity within a rock type or zone. For porosity, the highest CV in the hydraulic flow units (HFU) method is 0.65, observed in HFU11, while the lowest is 0.33, found in both HFU2 and HFU3. In the Winland method, the highest porosity CV is 0.53 in pore rock type 1, with the lowest at 0.33 in pore rock type 3. The Lorenz method shows the highest porosity CV at 0.61 in Zone Z5, and the lowest at 0.23 in Zone Z8 (Fig. 7).

Regarding permeability, the highest CV in the HFU method is 2.06 in HFU6, while the lowest is 0.38 in HFU5. The Winland method indicates the highest permeability CV of 1.13 in pore rock type 1, with the lowest at 0.58 in pore rock type 4. The Lorenz method reveals the highest permeability CV of 4.10 in Zone Z7, and the lowest at 0.86 in Zone Z9. For CV values of other zones, refer to Table 8.

4.3.2. Dykstra–Parson's coefficient (V_{DP})

The highest V_{DP} coefficient for porosity in the HFU method is 0.65, observed in HFU10, while the lowest value is 0.27, found in HFU2. In the Winland method, the highest V_{DP} coefficient for porosity is 0.57, associated with pore rock type 2, and the lowest value is 0.36, associated with pore rock type 6. According to the Lorenz method, the highest V_{DP} coefficient for porosity is 0.75 in Zone Z1, while the lowest value is 0.21 in Zone Z8 (Fig. 7).

For permeability, the highest V_{DP} coefficient in the HFU method is 0.92 in HFU7, with the lowest value at 0.70 in HFU2. In the Winland method, the highest permeability V_{DP} coefficient is 0.79 in pore rock type 1, while the lowest is 0.53 in pore rock type 3. The Lorenz method indicates the highest permeability V_{DP} coefficient at 0.93 in Zone Z6, with the lowest at 0.62 in Zone Z9. For further details and comparison of V_{DP} coefficients across other zones, refer to Table 8.

5. Discussion

This section discusses about the three key aspects of reservoir heterogeneity within the Sarvak Formation: their spatial scales, their origins, and their predictability. These factors are crucial for comprehending the distribution and quality of reservoir properties within the formation.

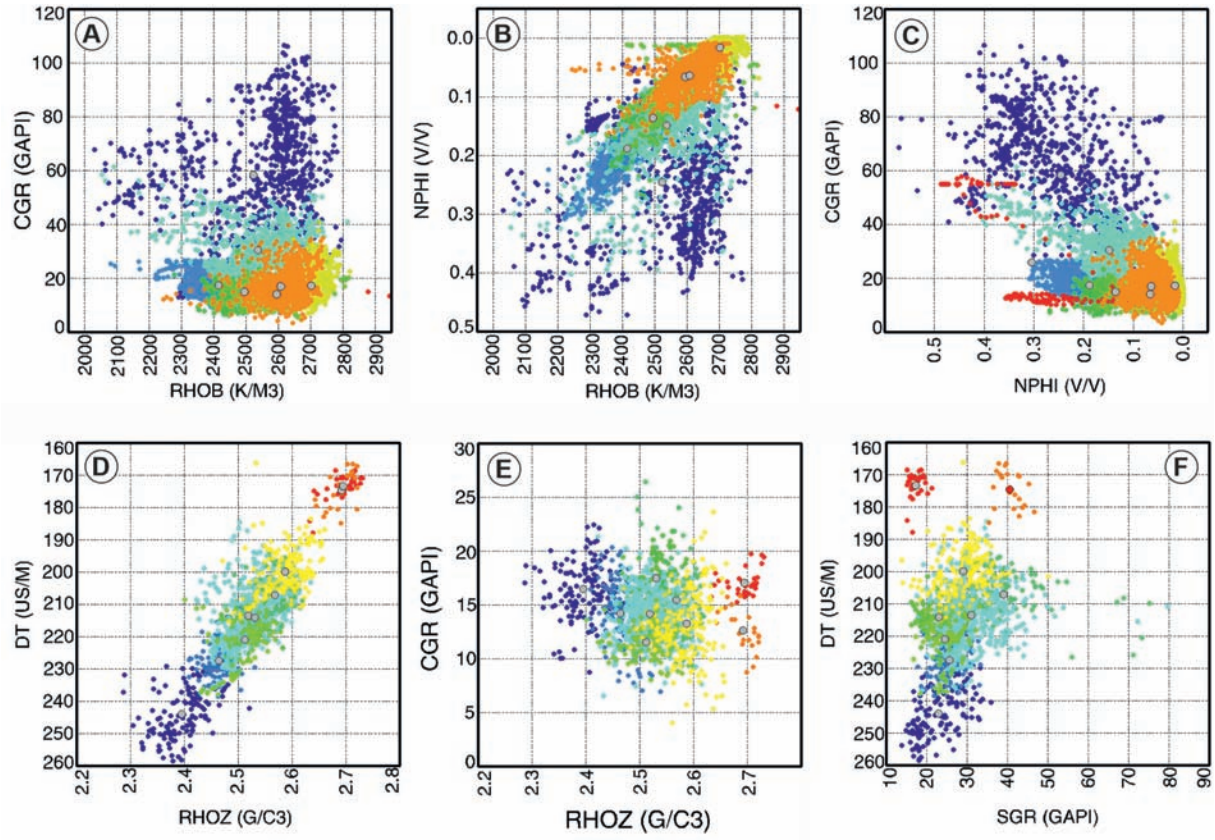


Fig. 6. Crossplots of petrophysical logs according to the identified electrofacies (EF) in the Sarvak Formation in the studied well-A (plots A to C) and well-B (plots D-F). A clear separation in data indicates reliable EF definition.

Table 7
Calculations of CV (coefficient of variation) and V_{DP} (Dykstra-Parsons) parameters for porosity values in HFU-9 of the Sarvak Fm. in the studied well-A.

Flow unit	Depth (m)	Porosity (%)	Porosity (v.v)	No.	Probability (%)
9	877.57	12.19	0.121	0	0
9	806.81	11.03	0.110	1	7.14
9	957.12	9.90	0.099	2	14.28
9	815.83	9.61	0.096	3	21.42
9	860.45	7.98	0.079	4	28.57
9	868.40	7.96	0.079	5	35.71
9	953.49	7.87	0.078	6	42.85
9	817.04	7.19	0.071	7	50
9	826.51	7.12	0.071	8	57.14
9	845.48	6.66	0.066	9	64.28
9	841.73	3.88	0.038	10	71.42
9	730.21	3.76	0.037	11	78.57
9	964.35	2.71	0.027	12	85.71
9	722.96	2.64	0.026	13	92.85
9	**945.70**	**2.58**	**0.025**	**14**	**100**
Probability (%)				**Porosity (%)**	**Permeability (mD)**
0.16	0.09904		**STDEVA**	3.14	202.25
0.5	0.0719		**Average**	6.87	164.26
0.84	0.0271		**CV**	0.45	1.23
Dykstra-Parsons (V_{DP}): 0.622					

5.1. Origin of reservoir heterogeneities

Heterogeneities in carbonate reservoirs are influenced by depositional and diagenetic processes, as well as by the presence of fractures (Ahr, 2008; Mehrabi and Bagherpour, 2022). Within the Sarvak Formation, these heterogeneities can be broadly classified into two primary categories: sedimentary heterogeneities and diagenetic heterogeneities. Sedimentary heterogeneities arise from variations in the textural attributes of sediments and sedimentary rocks, encompassing factors such as grain size, shape, sorting, compositional variations, sedimentary structures, and textural maturity (Abbasi et al., 2024; Tavoosi Iraj et al., 2021; Foroshani et al., 2023).

The Sarvak Formation exhibits a diverse suite of facies characterized by distinct textures, sizes, compositions, and sorting (MF1 to MF8 in Table 1). The interlayering and vertical

Table 8
Calculated CV (coefficient of variation) and V_{DP} (Dykstra-Parsons) parameters for porosity and permeability data in various hydraulic flow units (HFUs), Winland rock types (WRTs) and Lorenz zones in the Sarvak Formation, Abadan Plain, Zagros, Iran.

Method	Rock type/Zone code	Permeability (V_{DP})	Porosity (V_{DP})	Permeability (CV)	Porosity (CV)
HFU	**HFU1**	0.78	0.45	1.77	0.57
	HFU2	0.70	0.27	1.11	0.33
	HFU3	0.71	0.28	1.01	0.33
	HFU4	0.89	0.49	1.01	0.40
	HFU5	0.83	0.42	0.38	0.42
	HFU6	0.90	0.50	2.06	0.49
	HFU7	0.92	0.52	1.07	0.48
	HFU8	0.86	0.47	1.70	0.56
	HFU9	0.87	0.62	1.23	0.45
	HFU10	0.85	0.65	1.34	0.54
	HFU11	0.91	0.52	1.65	0.65
Winland	**WRT-1**	0.79	0.47	1.13	0.53
	WRT-2	0.72	0.57	0.85	0.49
	WRT-3	0.53	0.41	0.62	0.33
	WRT-4	0.55	0.41	0.58	0.38
	WRT-5	0.54	0.55	0.79	0.45
	WRT-6	0.56	0.36	0.87	0.47
	WRT-7	0.65	0.44	0.80	0.49
Lorenz	**Z1**	0.90	0.75	2.26	0.59
	Z2	0.67	0.48	2.14	0.44
	Z3	0.87	0.36	2.12	0.38
	Z4	0.90	0.39	2.86	0.34
	Z5	0.92	0.48	2.51	0.61
	Z6	0.93	0.49	2.60	0.54
	Z7	0.81	0.25	4.10	0.26
	Z8	0.80	0.21	1.98	0.23
	Z9	0.62	0.27	0.86	0.25
	Z10	0.85	0.56	3.12	0.49

arrangement of these facies, depending upon the prevailing depositional sub-environments and relative sea-level fluctuations, give rise to significant sedimentary heterogeneities. A prime example is the widespread occurrence of rudist facies (MF-7) with high reservoir potential within the upper parts of the formation. This heterogeneity is further accentuated by the interbedding of lagoonal mud-dominated facies (MF8), which exhibit poor reservoir quality, between these rudist-rich horizons. Similar heterogeneities, driven by lateral and vertical facies transitions, are observed throughout the Sarvak Formation in the studied field and across the Zagros area in SW Iran and the Persian Gulf (e.g., Kiani et al., 2022; Foroshani et al., 2023; Malekzadeh et al., 2020; Masoudi et al., 2012; Mehdipour et al., 2023, 2024).

Another indicator of sedimentary heterogeneity within the Sarvak Formation is the variability in the textural characteristics of grain-dominated, high-energy shoal facies (MF-4, MF-5). Variations in allochem size and sorting, coupled with the presence or absence of micrite, exert a significant influence on reservoir properties such as porosity and permeability (Deville de Periere et al., 2011). As a result, packstone and wackestone facies, typically developed in the landward portions of shoals and characterized by variable micrite content and poor sorting (MF6), generally exhibit lower reservoir quality compared to grainstone facies found in more seaward settings (MF4 and MF5).

Sedimentary structures, including cross-bedding, bioturbation, and graded bedding, further influence reservoir properties by controlling the direction of fluid flow (van den Berg, 2014). Cross lamination/bedding was frequently recorded within the high-energy shaol facies of MF4 and MF5. Bioturbation was dominantly recorded within the mud-supported lagoonal (MF8) and open marine (MF1 to MF3) settings. Oil and gas frequently migrate along bedding planes or laminations within facies exhibiting these features (Mehrabi et al., 2016; Nie et al., 2020).

While sedimentary processes lay the foundation for reservoir heterogeneity, diagenetic processes often significantly alter these initial characteristics, leading to substantial changes in reservoir quality (Ahr, 2008; Lucia, 2007; Moore, 2001). The complex diagenetic history of the Sarvak Formation has resulted in a substantial portion of its heterogeneities being attributed to diagenetic processes (Hajikazemi et al., 2017; Mehrabi, 2023; Taghavi et al., 2006; Yahyaei et al., 2025). Homogeneous reservoir horizons frequently develop beneath discontinuity surfaces (i.e., CT-ES and mT-ES), particularly below the Cenomanian–Turonian boundary, where extensive meteoric dissolution (karstification) has created large, interconnected cavities, thereby reducing reservoir heterogeneity (see *Section 4.1.2*). In contrast, extensive cementation within horizons located further away from these unconformities has significantly diminished reservoir quality (Fig. 4).

Dolomitization in the vicinity of pressure dissolution surfaces, such as stylolites and solution seams, has locally enhanced reservoir properties, particularly permeability, within dolomitized facies of the Sarvak Formation (Rahimpour-Bonab et al., 2012b). The stylolite-related dolomites are frequently recorded from the mud-dominated facies of middle to outer ramp settings (i.e., MF-1 to MF-3) and, with a lesser extent, in the lagoonal facies of MF-8. Furthermore, studies of drilling cores and thin sections from this formation have revealed the presence of both open and cemented fractures, which further influence the distribution of reservoir properties and contribute to diagenetic heterogeneities within the formation (Fig. 4) (see Ezati et al., 2018; Mazdarani et al., 2023).

5.2. Scale of reservoir heterogeneities

Heterogeneities in carbonate reservoirs exhibit a wide range of scales, and their accurate assessment is paramount for effective reservoir modeling (Tavakoli, 2020). In this study, the heterogeneities within the Sarvak Formation were investigated at two primary scales: small-scale (millimeter to centimeter) and large-scale (meter) variations.

- *Small-scale heterogeneities* were primarily characterized through detailed thin section analyses, which provide insights

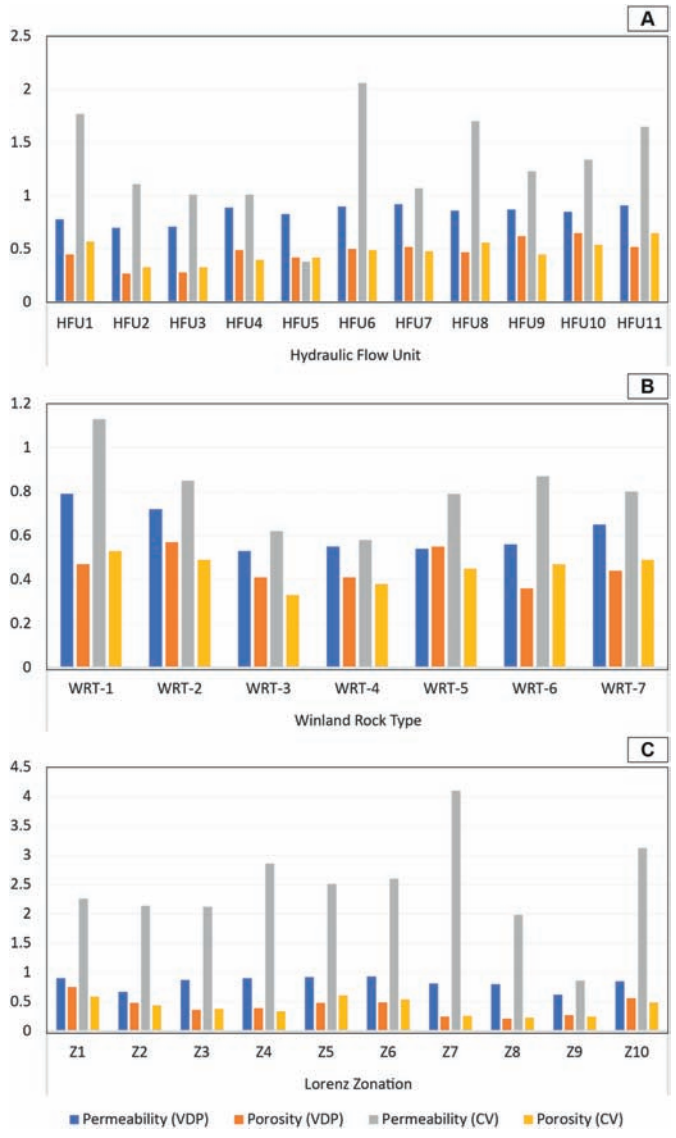


Fig. 7. Statistical plots of CV (coefficient of variation) and VDP (Dykstra-Parsons coefficient) values calculated for the hydraulic flow units (A), Winland rock types (B), and Lorenz zones (C) of the Sarvak Formation in the studied well-A. These plots are depicted for the porosity and permeability, separately.

into facies and diagenetic variations at fine-grained levels. The hydraulic flow unit (HFU) and Winland rock type (WRT) methodologies were employed to quantify these small-scale heterogeneities (see *sections 4.2.1 and 4.2.2*). Both approaches revealed substantial vertical heterogeneity within the Sarvak Formation (Fig. 8). Notably, the upper parts of the formation, particularly those underlying erosional unconformities, exhibited reduced diversity and increased homogeneity in reservoir rock types (Fig. 8). A comparative analysis of petrographic observations with HFU, WRT, and reservoir zonation (Tables 4 and 5) data indicated that these small-scale heterogeneities are primarily driven by variations in facies characteristics (sedimentary textures and structures) and the intensity of diagenetic processes (Mehrabi and Bagherpour, 2022). The most significant diagenetic processes affecting small-scale reservoir heterogeneities in the Sarvak Formation include mechanical and chemical compaction, early to late-stage calcite cementation, dolomitization, and fracturing. These processes exert considerable influence on pore network characteristics. For instance, grain-supported shoal facies are associated with distinct hydraulic flow units (HFUs), Winland rock types (WRTs), and electrofacies (EFs) due to their dominant diagenetic overprints. Highly cemented and compacted shoal facies display diminished reservoir quality, as evidenced by their classification within HFUs 1–3 (Table 3), WRTs 1 and 2 (Table 2), and EFs 5–7 (Table 5).

- For *large-scale heterogeneities*, the stratigraphically modified Lorenz zonation (SMLP) method proved to be the most effective approach (Gomes et al., 2008; Skalinski and Kenter, 2015). The identification of ten distinct zones with varying reservoir, baffle, and barrier properties underscored the presence of multiple large-scale heterogeneities within the Sarvak Formation (see *Section 4.2.3*) (Table 4). These large-scale heterogeneities can be attributed to two primary factors: lateral and vertical transitions of facies belts and diagenetic processes associated with erosional unconformities. A clear correlation exists between reservoir zones in the Sarvak Formation and paleoexposure surfaces, particularly in the upper portion of the formation (Fig. 8). The most productive reservoir zones (Zones 2 and 3; Fig. 8) exhibit the highest storage (PhiH: 15.85% for Zone 2 and 14.80% for Zone 3; Table 4) and flow (KH: 14.76% for Zone 2 and 24.28% for Zone 3; Table 4) capacities, which are predominantly located beneath the Cenomanian–Turonian boundary paleoexposure surface (CT-ES; Fig. 8). Within these zones, extensive meteoric dissolution played a key role in enhancing reservoir quality by homogenizing pore networks, as supported by calculated coefficient of variation (CV) and Dykstra-Parsons (V_{DP}) values (Table 8).

A comparison between the sedimentological log (Fig. 4) and reservoir quality evaluation log (Fig. 8) of the Sarvak Formation demonstrates that reservoir heterogeneities in the lower half of the formation (Zones 4 to 10; Fig. 8) are controlled by the interplay of depositional and diagenetic factors. The depositional facies vary from shallow-marine lagoonal (MF8) to shoal (MFs 4–6), reef-talus (MF7), and open-marine (MFs 1–3) environments, exhibiting both gradual and abrupt vertical transitions that contribute to large-scale heterogeneities (Figs. 4 and 8). Furthermore, late-stage diagenetic processes—including shallow-to-deep burial mechanisms such as blocky calcite cementation, compaction, recrystallization, dolomitization, and fracturing—significantly influenced reservoir properties in this interval (Fig. 4). Notably, extensive dolomitization along stylolites and solution seams has enhanced reservoir quality in Zones 7 and 10, as evidenced by their high storage (PhiH: 10.54% for Z7 and 10.75% for Z10; Table 4) and flow (KH: 7.29% for Z7 and 11.93% for Z10; Table 4) capacities (Fig. 8). Elevated reservoir heterogeneity levels across Zones 4 to 10 are further supported by their CV and V_{DP} coefficients (Table 8).

5.3. Predictability of reservoir heterogeneities

The integration of statistical analysis (CV and V_{DP}) with reservoir quality evaluations, coupled with sequence stratigraphic framework, demonstrates that large-scale heterogeneities within the Sarvak Formation are effectively traceable and predictable within the context of third-order sequences and systems tracts (Fig. 8).

Optimal reservoir horizons, such as rudist zones and dissolved shoal facies, are predominantly situated below the Cenomanian-Turonian sequence boundary (CT-ES), specifically within the regressive systems tract (RST) of the SV_Cen Sequence (Fig. 8). High-quality hydraulic flow units (HFUs 7 to 9), Winland rock types (WRTs 5 to 7) and electrofacies (EFs 1 to 4) are concentrated

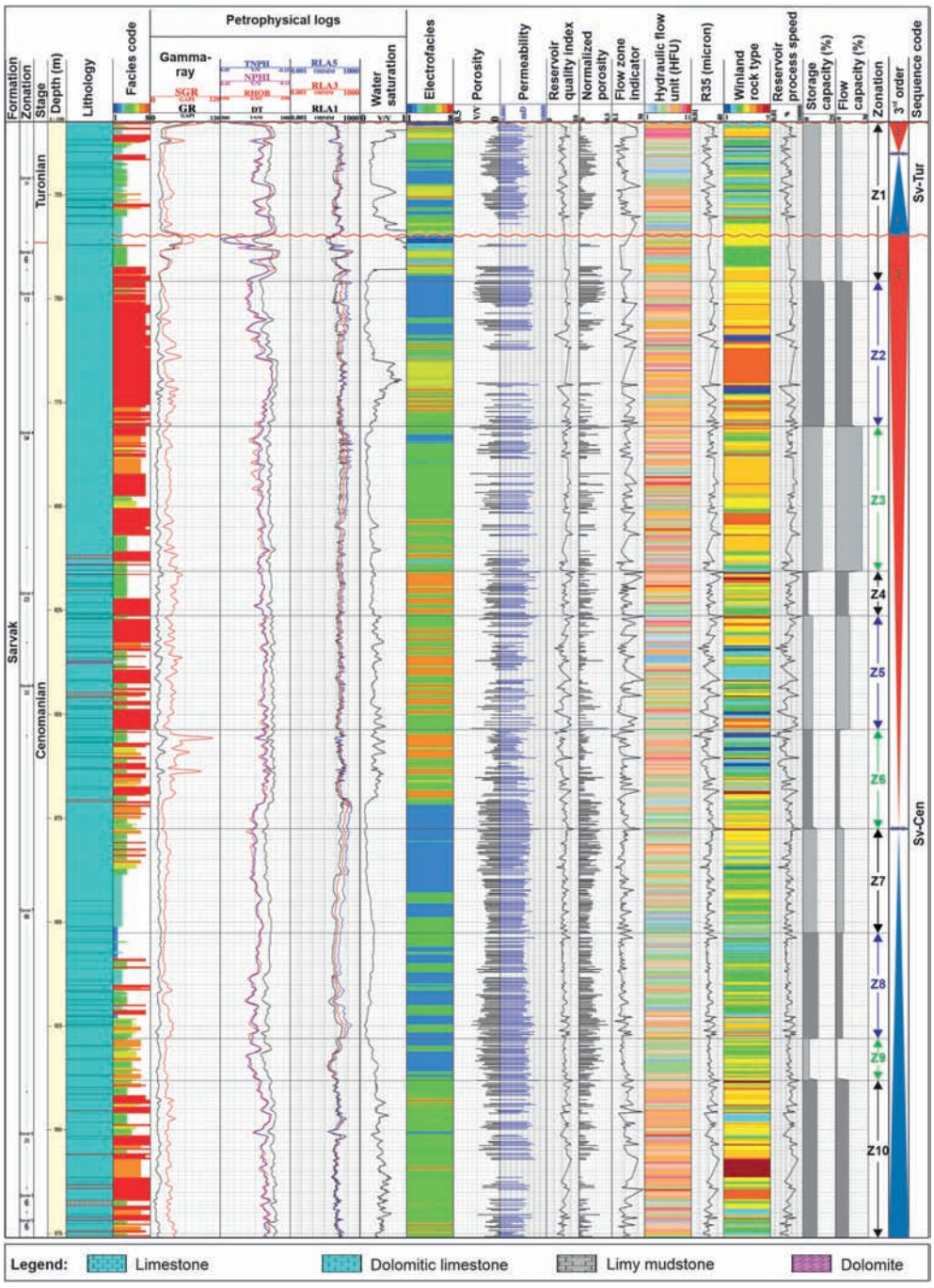


Fig. 8. Comprehensive reservoir quality log of the Sarvak Formation in the studied field in the Abadan Plain.

within the regressive systems tracts of third-order sequences, highlighting the strong influence of sequence stratigraphy on the distribution of reservoir properties (Cao et al., 2018; Magalhães et al., 2020). Within these karstified intervals, the presence of well-preserved dissolution vugs and channels points towards a relatively brief (less than one million year) subaerial exposure at the CT-ES, as corroborated by previous absolute dating studies (Navidtalab et al., 2016, 2024; Mehrabi et al., 2022a, 2022b). This short-lived exposure under a warm and humid (tropical) paleoclimate resulted in the development of a young karst profile (Sandhu et al., 2020; Veress, 2020), characterized by exceptional reservoir quality (i.e., high porosity and permeability) (Fig. 9A and B).

Conversely, medium to low-quality flow units (HFUs 1 to 6), reservoir rock types (WRTs 1 to 4) and electrofacies (EFs 5 to 7) are typically associated with transgressive systems tracts (TST) and are spatially distributed around maximum flooding surfaces (MFS), further emphasizing the stratigraphic control on reservoir heterogeneity (Fig. 8). Below the mT-ES, the prolonged (2–7 million years, according to previous absolute dating studies by Navidtalab et al., 2016, 2024; Mehrabi et al., 2022a, b) subaerial exposure led to the formation of an over-mature (senile) karst profile, characterized by the development of dissolution-collapsed brecciated units and, consequently, lower reservoir quality (Fig. 9A and B). Various types of karst breccias (Fig. 9C) have been identified within this part of the Sarvak Formation across the Zagros area,

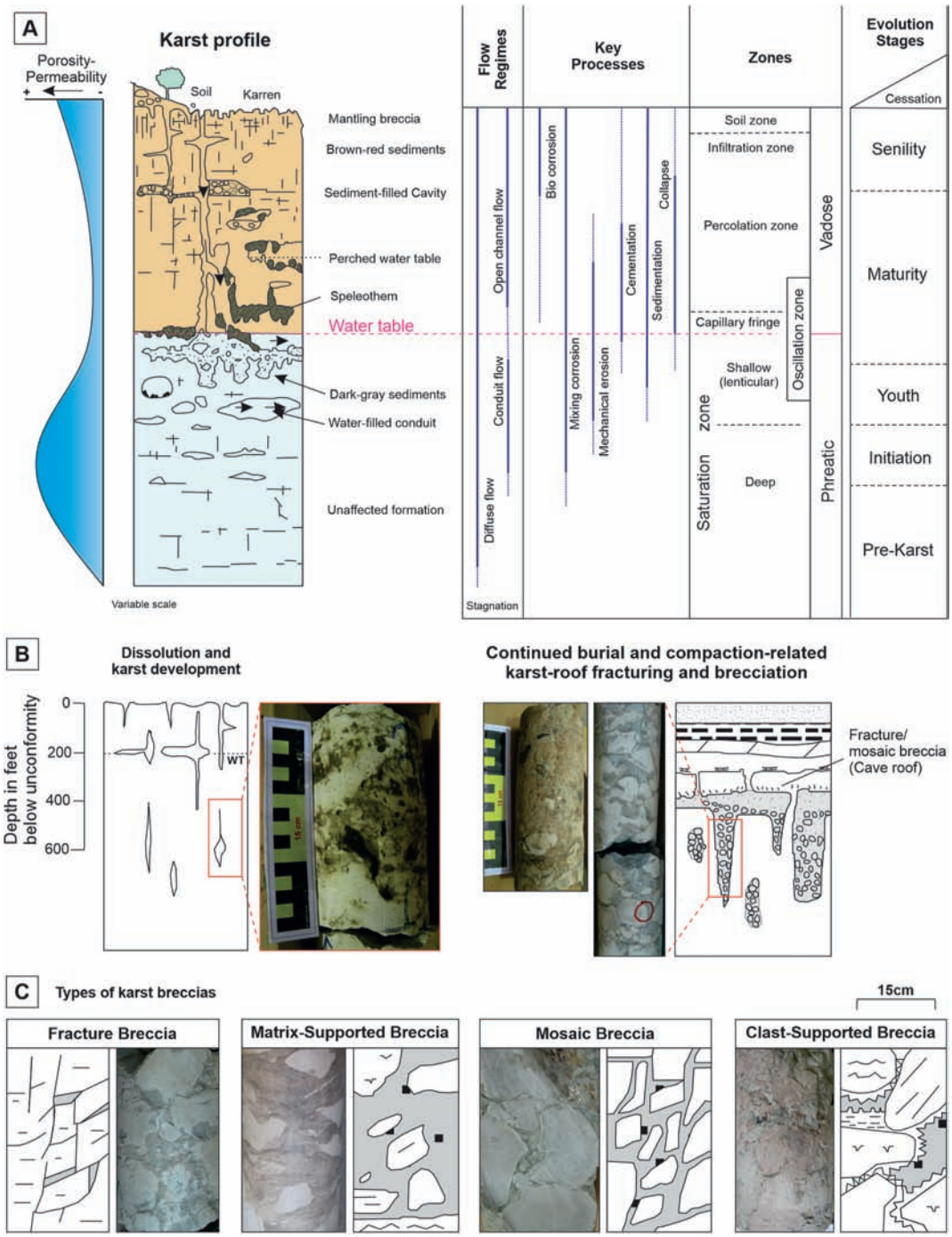


Fig. 9. A: An schematic cartoon illustaring the typical karst profile along with key processes, flow regimes and evolution stages (modified after Esteban and Klappa, 1983). B: Two scenarios of preserved (young) and collapsed-brecciated (senile) karst profile along with representative core photos from the Sarvak Formation. C: Various types of karst breccias recorded in the Sarvak Formation (cartoons adopted with some midifications from Kerans, 1990).

including the Dezful Embayment (Mehrabi and Rahimpour-Bonab, 2014; Rahimpour-Bonab et al., 2013), Fars (Bagherpour et al., 2021), and the Abadan Plain (Abbasi et al., 2024; Mehrabi et al., 2023a, 2024; Yahyaei et al., 2025).

Reservoir zonation based on Lorenz method delineates two significant reservoir intervals within the Sarvak Formation (Fig. 8):

Below the Cenomanian-Turonian Boundary: This interval represents the most productive reservoir within the Sarvak Formation (i.e., Z2 and Z3 in Fig. 8), characterized by the highest porosity (up to 30%) and permeability (exceeding 100 mD). It aligns with HFUs 7 to 11, WRTs 5 to 7 and EFs 1 to 4, corresponding to the regressive systems tract (RST) of the third-order Cenomanian sequence (Sv-Cen. in Fig. 8). The homogeneity measered by CV and V_{DP} indices within this zone is primarily attributed to extensive meteoric dissolution within the grain-dominated rudist facies (see *Section 4.3* and Table 8).

Below the mid-Turonian Unconformity: This reservoir interval (i.e., Z1 in Fig. 8) is relatively thinner and exhibits slightly lower reservoir quality compared to the interval below the Cenomanian-Turonian boundary (Fig. 8). The improved quality within this zone is primarily due to the presence of grain-dominated rudist facies and bioclastic grainstones of the shoal sub-environment, coupled with

limited meteoric dissolution. It corresponds to the regressive systems tract of the third-order Turonian sequence (Sv-Tur. in Fig. 8).

The study findings suggest that small-scale reservoir heterogeneities, primarily controlled by depositional processes such as variations in textural parameters, are not as effectively captured within the third-order sequence framework. A more detailed analysis, incorporating fourth- and fifth-order sequences or cycles, is necessary to effectively characterize these subtle variations and sedimentary cycles that influence small-scale reservoir characteristics.

The integration of sedimentological, petrophysical, and statistical approaches in this study has significantly advanced our understanding of the Sarvak Formation's reservoir heterogeneities. By combining facies analysis, diagenetic studies, and sequence stratigraphy with reservoir rock classification methods and statistical heterogeneity quantification, we have identified key controls on fluid flow and storage capacity that were previously overlooked. For instance, the application of the Coefficient of Variation and Dykstra–Parson's coefficient has provided a quantitative measure of heterogeneity, revealing distinct patterns that correlate with sedimentological and diagenetic features. This integrated approach has not only refined the characterization of hydraulic flow units and electrofacies but also highlighted the impact of diagenetic overprinting on reservoir quality. Consequently, our findings offer a more accurate and predictive model for reservoir heterogeneity in the Sarvak Formation, which can be applied to improve reservoir management and development strategies in the Abadan Plain and analogous carbonate reservoirs worldwide.

6. Conclusions

The study provides a thorough analysis of reservoir heterogeneities in the Sarvak Formation, considering depositional and diagenetic factors, as well as their influence on reservoir quality across different scales. The main conclusions are as follows:

- The study highlights the presence of reservoir heterogeneities within the Sarvak Formation at both large and small scales. Large-scale heterogeneities are primarily controlled by diagenetic processes, while small-scale heterogeneities are influenced by depositional processes, particularly changes in textural parameters.
- Large-scale heterogeneities, such as those associated with sequence stratigraphic boundaries, are predictable and traceable within the framework of third-order sequences and systems tracts. High-quality reservoir units, including rudist zones and dissolved shoal facies, are predominantly located below the Cenomanian-Turonian and mid-Turonian sequence boundaries.
- The identification of eleven hydraulic flow units (HFUs) and seven Winland rock types (WRTs) in the Sarvak Formation underscores the variability in reservoir quality. High-quality HFUs (7–9) and WRTs (5–7) are concentrated in regressive systems tracts, while lower-quality units are primarily found in transgressive systems tracts.
- Small-scale heterogeneities, driven by facies changes and diagenetic processes, are not well traceable within third-order sequences and require the use of lower-order sequences (fourth- and fifth-order) for accurate prediction.
- Diagenetic processes, including meteoric dissolution, cementation, and dolomitization, significantly impacted the reservoir properties of the Sarvak Formation. The study identifies areas of increased homogeneity associated with meteoric dissolution and reduced reservoir quality due to extensive cementation.
- The Sarvak Formation is divided into two key reservoir units based on sequence stratigraphy, with the best reservoir properties found below the Cenomanian-Turonian boundary. These zones show significant differences in porosity, permeability, and homogeneity, driven by both depositional and diagenetic factors.

Beneath the Cenomanian-Turonian exposure surface (CT-ES), short-lived subaerial exposure under warm, humid (tropical) paleoclimatic conditions fostered the development of a young karst profile exhibiting exceptional reservoir quality. In contrast, below the mid-Turonian exposure surface (mT-ES), prolonged subaerial exposure resulted in an over-mature (senile) karst profile. This mature profile is characterized by dissolution-collapsed brecciated units and paleosols, which correspond to diminished reservoir quality.

CRediT authorship contribution statement

Hamzeh Mehrabi: Writing – review & editing, Writing – original draft, Visualization, Validation, Supervision, Software, Resources, Methodology, Investigation, Conceptualization. **Rakhshandeh Ataei:** Writing – original draft, Software, Methodology, Investigation, Formal analysis, Data curation. **Vahid Tavakoli:** Writing – review & editing, Writing – original draft, Supervision, Methodology. **Elham Talebi:** Writing – original draft, Visualization, Validation, Software, Resources, Methodology, Investigation.

Data availability statement

Data will be made available on request.

Declaration of Generative AI and AI-assisted technologies in the writing process

During the preparation of this work, the author(s) used AI in order to improve the readability and language of the manuscript. After using this tool/service, the author(s) reviewed and edited the content as needed and take(s) full responsibility for the content of the published article.

Declaration of competing interest

The authors declare that they have no known competing financial interests or personal relationships that could have appeared to influence the work reported in this paper.

Acknowledgement

The authors express their gratitude to the University of Tehran for providing the facilities necessary for this research. The National Iranian Oil Company is thanked for data support. Journal editors and reviewers are thanked for their constructive comments and suggestions.

References

Abbasi, R., Mehrabi, H., Yahyaei, E., Rahimpour-Bonab, H., 2024. Diagenetic evolution of Upper Cretaceous carbonate sequences (Sarvak Formation) in the Abadan Plain, Iran: evidence from petrographic, elemental, stable, and strontium isotopic data. Int. Geol. Rev. 1–21. https://doi.org/10.1080/00206814.2024.2361276, 00(00.

Abdolahi, A., Bahrehvar, M., Mehrabi, H., Omidvar, M., Kadkhodaie, A., Wood, D. A., 2024. Paleoclimate changes across the Cenomanian–Santonian transition at the southern Neo-Tethys margin (SW Iran): An integrated approach. Gondwana Research 131, 208–236. https://doi.org/10.1016/j.gr.2024.02.013.

Ahr, W.M., 2008. Summary: geology of carbonate reservoirs. In: Ahr, W.M. (Ed.), Geology of Carbonate Reservoirs. John Wiley and Sons, Inc. https://doi.org/10.1002/9780470370650.ch8.

Alavi, M., 2004. Regional stratigraphy of the Zagros fold-thrust belt of Iran and its proforeland evolution. Am. J. Sci. 304 (1), 1–20. https://doi.org/10.2475/ajs.304.1.1.

Alsharhan, A.S., 2014. Petroleum systems in the Middle East. Geological Society 392 (1), 361–408. https://doi.org/10.1144/SP392.19. London, Special Publications.

Amaefule, J.O., Altunbay, M., Tiab, D., Kersey, D.G., Keelan, D., 1993. Enhanced Reservoir Description: Using Core and Log Data to Identify Hydraulic (Flow) Units and Predict Permeability in Uncored Intervals/Wells. *All Days*. https://doi.org/10.2118/26436-MS.

Aqrawi, A.A.M., Mahdi, T.A., Sherwani, G.H., Horbury, A.D., 2010. Characterisation of the Mid-Cretaceous Mishrif Reservoir of the southern Mesopotamian Basin, Iraq. In: AAPG GEO 2010 Middle East Geoscience Conference and Exhibition. Manama, Bahrain.

Asadi Mehmandosti, E., Adabi, M.H., Woods, A.D., 2013. Microfacies and geochemistry of the Middle Cretaceous Sarvak Formation in Zagros Basin, Izeh Zone, SW Iran. Sediment. Geol. 293, 9–20. https://doi.org/10.1016/j.sedgeo.2013.04.005.

Assadi, A., Honarmand, J., Moallemi, S.-A., Abdollahie-Fard, I., 2016. Depositional environments and sequence stratigraphy of the Sarvak Formation in an oil field in the Abadan Plain, SW Iran. Facies 62 (4), 26. https://doi.org/10.1007/s10347-016-0477-5.

Bagherpour, B., Mehrabi, H., Faghih, A., Vaziri-Moghaddam, H., Omidvar, M., 2021. Tectono-eustatic controls on depositional setting and spatial facies distribution of Coniacian–Santonian sequences of the Zagros Basin in Fars area, S. Iran. Mar. Petrol. Geol. 129. https://doi.org/10.1016/j.marpetgeo.2021.105072.

Bauer, J., Kuss, J., Steuber, T., 2002. Platform environments, microfacies and systems tracts of the upper Cenomanian-lower Santonian of Sinai, Egypt. Facies 47 (1), 1–25. https://doi.org/10.1007/BF02667703.

Bromhead, A.D., van Buchem, F.S.P., Simmons, M.D., Davies, R.B., 2022. Sequence stratigraphy, palaeogeography and petroleum plays of the Cenomanian–Turonian succession of the Arabian Plate: an updated synthesis. J. Petrol. Geol. 45 (2), 119–161. https://doi.org/10.1111/jpg.12810.

Cao, Z., Lin, C., Dong, C., Ren, L., Han, S., Dai, J., Xu, X., Qin, M., Zhu, P., 2018. Impact of sequence stratigraphy, depositional facies, diagenesis and CO2 charge on reservoir quality of the lower cretaceous Quantou Formation, Southern Songliao Basin, China. Mar. Petrol. Geol. 93, 497–519. https://doi.org/10.1016/j.marpetgeo.2018.03.015.

Catuneanu, O., Galloway, W.E., Kendall, C.G.S.C., Miall, A.D., Posamentier, H.W., Strasser, A., Tucker, M.E., 2011. Sequence stratigraphy: methodology and nomenclature. Newslett. Stratigr. 44, 173–245.

Cestari, R., Sartorio, D., 1995. Rudists and Facies of the Periadriatic Domain. Agip, p. 207.

Deville de Periere, M., Durlet, C., Vennin, E., Lambert, L., Bourillot, R., Caline, B., Poli, E., 2011. Morphometry of micrite particles in cretaceous microporous limestones of the Middle East: influence on reservoir properties. Mar. Petrol. Geol. 28 (9), 1727–1750. https://doi.org/10.1016/j.marpetgeo.2011.05.002.

di Stefano, P., Ruberti, D., 2000. Cenomanian rudist-dominated shelf-margin limestones from the panormide carbonate platform (Sicily, Italy): facies analysis and sequence stratigraphy. Facies 42 (1), 133–160. https://doi.org/10.1007/BF02562570.

Dunham, R.J., 1962. Classification of carbonate rocks according to depositional textures. Classification of Carbonate Rocks–A Symposium, pp. 108–121.

Elkateb, T., Chalaturnyk, R., Robertson, P.K., 2003. An overview of soil heterogeneity: quantification and implications on geotechnical field problems. Can. Geotech. J. 40 (1), 1–15.

Embry, A.F., 2002. Transgressive-regressive (TR) sequence stratigraphy. In: Gulf Coast SEPM Conference Proceedings, pp. 151–172 (Houston).

Embry, A.F., Klovan, J.E., 1971. A Late Devonian reef tract on northeastern Banks Island, NWT. Bull. Can. Petrol. Geol. 19 (4), 730–781. http://archives.datapages.com/data/cspg/data/019/019004/0730.htm.

Enayati–Bidgoli, A.H., Rahimpour–Bonab, H., 2016. A geological based reservoir zonation scheme in a sequence stratigraphic framework: a case study from the Permo–Triassic gas reservoirs, Offshore Iran. Mar. Petrol. Geol. 73 (4).

Esrafili-Dizaji, B., Rahimpour-Bonab, H., Mehrabi, H., Afshin, S., Kiani Harchegani, F., Shahverdi, N., 2015. Characterization of rudist-dominated units as potential reservoirs in the middle Cretaceous Sarvak Formation, SW Iran. Facies 61 (3). https://doi.org/10.1007/s10347-015-0442-8.

Esteban, M., Klappa, C.F., 1983. In: Scholle, P.A., Bebout, D.G., Moore, C.H. (Eds.), Carbonate Depositional Environments in Subaerial Exposure Environment, 33. AAPG Mem, p. 708.

Ezati, M., Azizzadeh, M., Riahi, M.A., Fattahpour, V., Honarmand, J., 2018. Characterization of micro-fractures in carbonate Sarvak reservoir, using petrophysical and geological data, SW Iran. J. Petrol. Sci. Eng. 170, 675–695. https://doi.org/10.1016/j.petrol.2018.06.058.

Fitch, P.J.R., Lovell, M.A., Davies, S.J., Pritchard, T., Harvey, P.K., 2015. An integrated and quantitative approach to petrophysical heterogeneity. Mar. Petrol. Geol. 63, 82–96. https://doi.org/10.1016/j.marpetgeo.2015.02.014.

Flügel, E., 2013. Microfacies of Carbonate Rocks. Springer. https://doi.org/10.1007/978-3-662-08726-8.

Foroshani, J.S., Mehrabi, H., Rahimpour-Bonab, H., 2023. Reservoir heterogeneity of Upper Cretaceous Sarvak Formation in the Dezful Embayment, SW Iran: Implications of flow unit distribution, electrofacies analysis and geological-based reservoir zonation. Journal of African Earth Sciences 200, 104882. https://doi.org/10.1016/j.jafrearsci.2023.104882.

Fragoso, G.C.D., Henrique de Melo, A., Arienti Gonçalves, L., Brandão Bunevich, R., de Aratanha Maia Araujo, J., Camanho da Costa, T., Alexandre Pedrosa, C., Marlon Dos Santos Scherer, C., 2023. High-resolution sequence stratigraphy applied to reservoir characterization of the Brazilian Cretaceous pre-salt section, Campos Basin: guidelines for geological modeling and reservoir management. Mar. Petrol. Geol. 151, 106203. https://doi.org/10.1016/j.marpetgeo.2023.106203.

Gholami Zadeh, P., Adabi, M.H., Sadeghi, A., 2019. Microfacies, geochemistry and sequence stratigraphy of the Sarvak Formation (Mid Cretaceous) in the Kuh-e Siah and Kuh-e Mond, Fars area, southern Iran. J. Afr. Earth Sci. 160, 103634. https://doi.org/10.1016/j.jafrearsci.2019.103634.

Gomes, J.S., Ribeiro, M.T., Strohmenger, C.J., Negahban, S., Kalam, M.Z., 2008. Carbonate reservoir rock typing – the Link between geology and SCAL. All Days. https://doi.org/10.2118/118284-MS.

Gunter, G.W., Finneran, J.M., Hartmann, D.J., Miller, J.D., 1997. Early determination of reservoir flow units using an integrated petrophysical method. In: Proceedings - SPE Annual Technical Conference and Exhibition, pp. 373–380. https://doi.org/10.2118/38679-ms. Omega(Pt 1.

Hajikazemi, E., Al-Aasm, I.S., Coniglio, M., 2010. Subaerial Exposure and Meteoric Diagenesis of the Cenomanian-Turonian Upper Sarvak Formation, Southwestern Iran, 330. Geological Society Special Publication, pp. 253–272. https://doi.org/10.1144/SP330.12.

Hajikazemi, E., Al-Aasm, I.S., Coniglio, M., 2012. Chemostratigraphy of cenomanian-turonian carbonates of the sarvak formation, Southern Iran. J. Petrol. Geol. 35 (2), 187–205. https://doi.org/10.1111/j.1747-5457.2012.00525.x.

Hajikazemi, E., Al-Aasm, I.S., Coniglio, M., 2017. Diagenetic history and reservoir properties of the Cenomanian-Turonian carbonates in southwestern Iran and the Persian Gulf. Mar. Pet. Geol. 88, 845–857. https://doi.org/10.1016/j.marpetgeo.2017.06.035.

Hollis, C., 2011. Diagenetic controls on reservoir properties of carbonate successions within the Albian-Turonian of the Arabian Plate. Pet. Geosci. 17 (3), 223–241. https://doi.org/10.1144/1354-079310-032.

Hosseinzadeh, M., Tavakoli, V., 2024. Analyzing the impact of geological features on reservoir heterogeneity using heterogeneity logs: a case study of Permian reservoirs in the Persian Gulf. Geoenergy Sci. Eng. 237, 212810. https://doi.org/10.1016/j.geoen.2024.212810.

Jafarian, A., Kakemem, U., Husinec, A., Mehrabi, H., Javanbakht, M., Wang, C., Chen, X., Li, Y., 2024. Depositional facies and diagenetic control on reservoir quality of the Aptian Dariyan Formation, NW Persian Gulf. Marine and Petroleum Geology 165, 106895. https://doi.org/10.1016/j.marpetgeo.2024.106895.

Johnson, C.E., 1956. Prediction of oil recovery by waterflood - a simplified graphical treatment of the Dykstra-Parsons method. J. Petrol. Technol. 8 (11), 55–56. https://doi.org/10.2118/733-g.

Kalanat, B., Vaziri-Moghaddam, H., Bijani, S., 2021. Depositional history of the uppermost Albian–Turonian Sarvak Formation in the Izeh Zone (SW Iran). Int. J. Earth Sci. 110 (1), 305–330. https://doi.org/10.1007/s00531-020-01954-1.

Keller, G., 2008. Cretaceous climate, volcanism, impacts, and biotic effects. Cretac. Res. 29 (5–6), 754–771. https://doi.org/10.1016/j.cretres.2008.05.030.

Kerans, C., 1990. Depositional systems and karst geology of the Ellenburger Group (Lower Ordovician), subsurface West Texas: Bur. Econ. Geol. Univ. Texas. Rept. Invest. 193, 63.

Kiani, A., Saberi, M.H., ZareNezhad, B., Mehmandosti, E.A., 2022. Reservoir zonation in the framework of sequence stratigraphy: a case study from Sarvak Formation, Abadan Plain, SW Iran. J. Petrol. Sci. Eng. 208, 109560. https://doi.org/10.1016/j.petrol.2021.109560.

Kolodzie, S., 1980. Analysis of pore throat size and use of the Waxman-Smits equation to determine OOIP in spindle field. In: Colorado, SPE. Society of Petroleum Engineers of AIME. https://doi.org/10.2523/9382-ms.

Korbar, T., Fuček, L., Husinec, A., Vlahović, I., Oštrić, N., Matičec, D., Jelaska, V., 2001. Cenomanian carbonate facies and rudists along shallow intraplatform basin margin-the island of Cres (Adriatic Sea, Croatia). Facies 45 (1), 39–58. https://doi.org/10.1007/BF02668104.

Lake, L.W., Jensen, J.L., 1991. A review of heterogeneity measures used in reservoir characterization. In Situ 15 (4), 409–440.

Lucia, F., 2007. Carbonate Reservoir Characterization. Springer-Verlag, Berlin, p. 341. https://doi.org/10.2118/82071-ms.

Madanipour, S., Najafi, M., Nozaem, R., Vergés, J., Yassaghi, A., Heydari, I., Khodaparast, S., Soudmand, Z., Aghajari, L., 2024. The Arabia – Eurasia collision zone in Iran: tectonostratigraphic and structural synthesis. J. Petrol. Geol. 47 (2), 123–171. https://doi.org/10.1111/jpg.12854.

Magalhães, A.J.C., Raja Gabaglia, G.P., Fragoso, D.G.C., Bento Freire, E., Lykawka, R., Arregui, C.D., Silveira, M.M.L., Carpio, K.M.T., de Gasperi, A., Pedrinha, S., Artagão, V.M., Terra, G.J.S., Bunevich, R.B., Roemers-Oliveira, E., Gomes, J.P., Hernández, J.I., Hernández, R.M., Bruhn, C.H.L., 2020. High-resolution sequence stratigraphy applied to reservoir zonation and characterisation, and its impact on production performance - shallow marine, fluvial downstream, and lacustrine carbonate settings. Earth Sci. Rev. 210, 103325. https://doi.org/10.1016/j.earscirev.2020.103325.

Malekzadeh, H., Daraei, M., Bayet-Goll, A., 2020. Field-scale reservoir zonation of the Albian–Turonian Sarvak Formation within the regional-scale geologic framework: a case from the Dezful Embayment, SW Iran. Mar. Petrol. Geol. 121, 104586. https://doi.org/10.1016/j.marpetgeo.2020.104586.

Masoudi, P., Tokhmechi, B., Bashari, A., Jafari, M.A., 2012. Identifying productive zones of the Sarvak formation by integrating outputs of different classification methods. J. Geophys. Eng. 9 (3), 282–290. https://doi.org/10.1088/1742-2132/9/3/282.

Mazdarani, A., Kadkhodaie, A., Wood, D.A., Soluki, Z., 2023. Natural fractures characterization by integration of FMI logs, well logs and core data: a case study from the Sarvak Formation (Iran). J. Pet. Explor. Prod. Technol. 13 (5), 1247–1263. https://doi.org/10.1007/s13202-023-01611-8.

Mehdipour, V., Rabbani, A.R., Kadkhodaie, A., 2023. Geological modeling of diagenetic logs of the Sarvak reservoir in Dezful Embayment, southwestern Iran: implications for geostatistical simulation and reservoir quality assessment. J. Pet. Explor. Prod. Technol. 13 (10), 2083–2107. https://doi.org/10.1007/s13202-023-01670-x.

Mehdipour, V., Rabbani, A.R., Kadkhodaie, A., 2024. Quantitative analysis of diagenesis control on the spatial heterogeneity of Sarvak Carbonate Formation, the Dezful Embayment of Zagros Basin, western Iran. SPE J. 29 (6), 3118–3130. https://doi.org/10.2118/219742-PA.

Mehrabi, H., 2023. Deposition, diagenesis, and geochemistry of upper cretaceous carbonates (Sarvak Formation) in the Zagros Basin and the Persian Gulf, Iran. Minerals 13 (8), 1078. https://doi.org/10.3390/min13081078.

Mehrabi, H., Bagherpour, B., 2022. Scale, origin, and predictability of reservoir heterogeneities in shallow-marine carbonate sequences: a case from Cretaceous of Zagros, Iran. J. Petrol. Sci. Eng. 214, 110571. https://doi.org/10.1016/j.petrol.2022.110571.

Mehrabi, H., Rahimpour-Bonab, H., 2014. Paleoclimate and tectonic controls on the depositional and diagenetic history of the cenomanian-early Turonian carbonate reservoirs, Dezful Embayment, SW Iran. Facies 60 (1), 147–167. https://doi.org/10.1007/s10347-013-0374-0.

Mehrabi, H., Rahimpour-Bonab, H., Hajikazemi, E., Jamalian, A., 2015. Controls on depositional facies in Upper Cretaceous carbonate reservoirs in the Zagros area and the Persian Gulf, Iran. Facies 61 (4). https://doi.org/10.1007/s10347-015-0450-8.

Mehrabi, H., Bagherpour, B., Honarmand, J., 2020. Reservoir quality and micrite textures of microporous intervals in the Upper Cretaceous successions in the Zagros area, SW Iran. J. Petrol. Sci. Eng. 192. https://doi.org/10.1016/j.petrol.2020.107292.

Mehrabi, H., Amin, N., Eanayati-Bidgoli, A., Bagherpour, B., 2022a. Age, duration, and geochemical signatures of paleo-exposure events in Cenomanian–Santonian sequences (Sarvak and Ilam Formations) in SW Iran: insights from carbon and strontium isotopes chemostratigraphy. Sediment. Geol. 434, 106136. https://doi.org/10.1016/j.sedgeo.2022.106136.

Mehrabi, H., Mansouri, M., Rahimpour-Bonab, H., Tavakoli, V., Hassanzadeh, M., 2016. Chemical compaction features as potential barriers in the Permian-Triassic reservoirs of Southern Iran. Journal of Petroleum Science and Engineering 145, 95–113. https://doi.org/10.1016/j.petrol.2016.03.020.

Mehrabi, H., Navidtalab, A., Rahimpour-Bonab, H., Heimhofer, U., 2022b. Geochemical expression of sequence stratigraphic surfaces: a case from upper cretaceous shallow-water carbonates of southeastern Neo-Tethys margin, SW Iran. Cretac. Res. 140, 105329. https://doi.org/10.1016/j.cretres.2022.105329.

Mehrabi, H., Yahyaei, E., Navidtalab, A., Rahimpour-Bonab, H., Abbasi, R., Omidvar, M., Assadi, A., Honarmand, J., 2023a. Depositional and diagenetic controls on reservoir properties along the shallow-marine carbonates of the Sarvak Formation, Zagros Basin: petrographic, petrophysical, and geochemical evidence. Sediment. Geol. 454, 106457. https://doi.org/10.1016/j.sedgeo.2023.106457.

Mehrabi, H., Karami, F., Fakhar-Shahreza, N., Honarmand, J., 2023b. Pore-type characterization and reservoir zonation of the Sarvak Formation in the Abadan Plain, Zagros Basin, Iran. Minerals 13, 1464. https://doi.org/10.3390/min13121464.

Mehrabi, H., Fakhar-Shahreza, N., Karami, F., Honarmand, J., 2024. Controls of tectonics and paleoclimate on depositional–diagenetic evolution and pore types of Upper Cretaceous successions (Sarvak Formation) in the Abadan plain, Iran. Mar. Petrol. Geol. 170, 107118. https://doi.org/10.1016/j.marpetgeo.2024.107118.

Mohseni, H., Zeybaram Javanmard, R., 2020. New data on sequence stratigraphy of the Sarvak Formation in Malekshahi city, (Ilam province) Zagros basin, Iran. Mar. Petrol. Geol. 112, 104035. https://doi.org/10.1016/j.marpetgeo.2019.104035.

Moore, C., 2001. Carbonate Reservoirs Porosity Evolution and Diagenesis in a Sequence Stratigraphic Framework. Elsevier. https://doi.org/10.1016/s0264-8172(03)00037-0.

Moore, C.H., Wade, W.J., 2013. Carbonate diagenesis. Dev. Sedimentol. 67, 67–89. https://doi.org/10.1016/B978-0-444-53831-4.00005-7.

Motiei, H., 1993. Stratigraphy of Zagros. Treatise on the Geology of Iran 1, 60–151.

Navidtalab, A., Rahimpour-Bonab, H., Huck, S., Heimhofer, U., 2016. Elemental geochemistry and strontium-isotope stratigraphy of Cenomanian to Santonian neritic carbonates in the Zagros Basin, Iran. Sediment. Geol. 346, 35–48. https://doi.org/10.1016/j.sedgeo.2016.10.003.

Navidtalab, A., Mehrabi, H., Shafaii Moghadam, H., Rahimpour-Bonab, H., 2024. Strontium isotope proxy of sedimentological records reveals uplift and erosion in the Southeastern Neo-Tethys ocean during the late Cretaceous. Sci. Rep. 14 (1), 3499. https://doi.org/10.1038/s41598-024-54128-3.

Nie, H., Li, D., Liu, G., Lu, Z., Hu, W., Wang, R., Zhang, G., 2020. An overview of the geology and production of the Fuling shale gas field, Sichuan Basin, China. Energy Geoscience 1 (3–4), 147–164. https://doi.org/10.1016/j.engeos.2020.06.005.

Omidvar, M., Mehrabi, H., Sajjadi, F., Bahramizadeh-Sajjadi, H., Rahimpour-Bonab, H., Ashrafzadeh, A., 2014. Revision of the foraminiferal biozonation scheme in Upper Cretaceous carbonates of the Dezful Embayment, Zagros, Iran: integrated palaeontological, sedimentological and geochemical investigation. Rev. Micropaleontol. 57 (3), 97–116. https://doi.org/10.1016/j.revmic.2014.04.002.

Rabiller, P., 2005. Facies prediction and data modeling for reservoir characterization. FACIMAGE^{TM} methodology. In: Illustrated User's Guide of Geolog Software 6.6.1 to Geolog 6.7^{TM}. Prepared by Rabiller Edited, Rabiller Geo-consulting.

Rahimpour-Bonab, H., Mehrabi, H., Enayati-Bidgoli, A.H., Omidvar, M., 2012a. Coupled imprints of tropical climate and recurring emergence on reservoir evolution of a mid Cretaceous carbonate ramp, Zagros Basin, southwest Iran. Cretac. Res. 37, 15–34. https://doi.org/10.1016/j.cretres.2012.02.012.

Rahimpour-Bonab, H., Mehrabi, H., Navidtalab, A., Omidvar, M., Enayati-Bidgoli, A. H., Sonei, R., Sajjadi, F., Amiri-Bakhtyar, H., Arzani, N., Izadi-Mazidi, E., 2013. Palaeo-exposure surfaces in Cenomanian - Santonian carbonate reservoirs in the dezful embayment, SW Iran. J. Petrol. Geol. 36 (4), 335–362. https://doi.org/10.1111/jpg.12560.

Rahimpour-Bonab, H., Mehrabi, H., Navidtalab, A., Izadi-Mazidi, E., 2012b. Flow unit distribution and reservoir modelling in Cretaceous carbonates of the Sarvak Formation, *Abteymour* Oilfield, Dezful Embayment, SW Iran. J. Petrol. Geol. 35 (3), 213–236. https://doi.org/10.1111/j.1747-5457.2012.00527.x.

Razin, P., Taati, F., van Buchem, F.S.P., 2010. Sequence stratigraphy of Cenomanian-Turonian carbonate platform margins (Sarvak Formation) in the high Zagros, SW Iran: an outcrop reference model for the Arabian plate. In: van Buchem, F.S. P., Gerdes, K.D., Esteban, M. (Eds.), Mesozoic and Cenozoic Carbonate Systems of the Mediterranean and the Middle East: Stratigraphic and Diagenetic Reference Models. Geological Society of London, Special Publication.

Sadeghi, R., Moussavi-Harami, R., kadkhodaie, A., Mahboubi, A., Ashtari, A., 2021. Reservoir rock typing of the Asmari Formation using integrating geological and petrophysical data for unraveling the reservoir heterogeneity: a case study from the Ramshir oilfield, southwest Iran. Carbonates Evaporites 36 (3), 60. https://doi.org/10.1007/s13146-021-00692-y.

Sadooni, F.N., 2005. The nature and origin of Upper Cretaceous basin-margin rudist buildups of the Mesopotamian Basin, southern Iraq, with consideration of possible hydrocarbon stratigraphic entrapment. Cretac. Res. 26 (2), 213–224. https://doi.org/10.1016/j.cretres.2004.11.016.

Sadooni, F.N., Aqrawi, A.A.M., 2000. Cretaceous sequence stratigraphy and petroleum potential of the Mesopotamian Basin, Iraq. In: Middle East Models of Jurassic/Cretaceous Carbonate System. SEPM (Society for Sedimentary Geology). https://doi.org/10.2110/pec.00.69.0315.

Sandhu, D., Singh, A., Wang, D., 2020. Can we infer the age of karst conduit from the profile of potentiometric surface? J. Hydrol. 584, 124679. https://doi.org/10.1016/j.jhydrol.2020.124679.

Sharland, P.R., Archer, D.M., Casey, R.B., Davies, S.H., Hall, A.P., Heward, A.D., Horbury, A.D., Simmons, M.D., 2001. Arabian plate sequence stratigraphy. GeoMarine Special Publications (Chapter 4), 56–74, 2, 3.

Sharp, I., Gillespie, P., Morsalnezhad, D., Taberner, C., Karpuz, R., Verge's, J., Horbury, A., Pickard, N., Garland, J., Hunt, D., 2010. Stratigraphic architecture and fracture controlled dolomitization of the Cretaceous Khami and Bangestan groups: an outcrop case study, Zagros Mountains, Iran. In: van Buchem, F., Gerdes, K., Esteban, M. (Eds.), Mesozoic and Cenozoic Carbonate Systems of the Mediterranean and the Middle East: Stratigraphic and Diagenetic Reference Models, 329. Geological Society, London, Special Publication, pp. 343–396.

Sherkati, S., Letouzey, J., 2004. Variation of structural style and basin evolution in the central Zagros (Izeh zone and Dezful Embayment), Iran. Mar. Petrol. Geol. 21 (5), 535–554. https://doi.org/10.1016/j.marpetgeo.2004.01.007.

Simmons, M.D., Bidgood, M.D., Davies, R.B., Droste, H., Levell, B., Razin, P., van Buchem, F.S.P., 2025. Intra-Turonian stratigraphic reorganization on the Arabian Plate. Geological Society, London, Special Publications 545 (1). https://doi.org/10.1144/SP545-2023-207.

Skalinski, M., Kenter, J.A.M., 2015. Carbonate petrophysical rock typing: integrating geological attributes and petrophysical properties while linking with dynamic behaviour. Geological Society, London, Special Publications 406 (1), 229–259. https://doi.org/10.1144/SP406.6.

Song, H., Du, S., Wang, R., Wang, J., Wang, Y., Wei, C., Liu, Q., 2020. Potential for vertical heterogeneity prediction in reservoir basing on machine learning methods. Geofluids 2020, 1–12. https://doi.org/10.1155/2020/3713525.

Spalluto, L., 2012. Facies evolution and sequence chronostratigraphy of a "mid"-Cretaceous shallow-water carbonate succession of the Apulia Carbonate Platform from the northern Murge area (Apulia, southern Italy). Facies 58 (1), 17–36. https://doi.org/10.1007/s10347-011-0266-0.

Taghavi, A.A., Mørk, A., Emadi, M.A., 2006. Sequence stratigraphically controlled diagenesis governs reservoir quality in the carbonate Dehluran Field, southwest Iran. Pet. Geosci. 12 (2), 115–126. https://doi.org/10.1144/1354-079305-672.

Tavakoli, V., 2020. Microscopic Heterogeneity. Carbonate Reservoir Heterogeneity. Springer.

Tavoosi Iraj, P., Mehrabi, H., Rahimpour-Bonab, H., Ranjbar-Karami, R., 2021. Quantitative analysis of geological attributes for reservoir heterogeneity assessment in carbonate sequences; a case from Permian–Triassic reservoirs of the Persian Gulf. J. Petrol. Sci. Eng. 200, 108356. https://doi.org/10.1016/j.petrol.2021.108356.

Tiab, D., Donaldson, E.C., 2015. Petrophysics: Theory and Practice of Measuring Reservoir Rock and Fluid Transport Properties. Gulf Professional Publishing, pp. 1–889. https://doi.org/10.1016/B978-0-7506-7711-0.X5000-2.

Tucker, M.E., Wright, V.P., 1990. Carbonate Sedimentology. Blackwell, Oxford, p. 482. https://doi.org/10.1002/9781444314175.
van Buchem, F.S.P., Simmons, M.D., Droste, H.J., Davies, R.B., 2011. Late Aptian to Turonian stratigraphy of the eastern Arabian Plate e depositional sequences and lithostratigraphic nomenclature. Pet. Geosci. 17, 211–222.
van den Berg, J.H., 2014. Ebook - Sedimentary Structures and Their Relation to Bedforms and Flow Conditions. EAGE Publications bv. https://doi.org/10.3997/9789462820180.
Veress, M., 2020. Karst types and their karstification. J. Earth Sci. 31 (3), 621–634. https://doi.org/10.1007/s12583-020-1306-x.
Vergés, J., Casini, G., Ruh, J., Cosgrove, J., Sherkati, S., Najafi, M., Casciello, E., Saura, E., Fard, I.A., Piryaei, A., de Lamotte, D.F., Letouzey, J., Goodarzi, H., Soleimany, B., Jahani, S., 2024. Structural style and timing of nw-se trending Zagros folds in SW Iran: interaction with north-south trending Arabian folds and implications for petroleum geology. J. Petrol. Geol. 47 (1), 3–73. https://doi.org/10.1111/jpg.12850.
Xiao, Z., Ding, W., Hao, S., Wang, Z., Xu, C., Gao, H., Zhang, X., 2022. Quantitative evaluation of reservoir heterogeneity in the Ordos Basin based on Tamura texture features. Front. Earth Sci. 10. https://doi.org/10.3389/feart.2022.922608.
Yahyaei, E., Mehrabi, H., Abbasi, R., 2025. Isotopic and sedimentologic proxies of palaeoexposure events and oceanic anoxic event 2 (<scp>OAE2</scp>) in the Cenomanian–Turonian neritic carbonates (the Sarvak Formation) in the Abadan Plain, Zagros Basin, Iran. Geol. J. https://doi.org/10.1002/gj.5089.
Zahid, M.A., Chunmei, D., Lin, C., Gluyas, J., Jones, S., Zhang, X., Munawar, M.J., Ma, C., 2016. Sequence stratigraphy, sedimentary facies and reservoir quality of Es4s, southern slope of Dongying Depression, Bohai Bay Basin, East China. Mar. Petrol. Geol. 77, 448–470. https://doi.org/10.1016/j.marpetgeo.2016.06.026.